PFS: The Planetary Fourier Spectrometer

V. Formisano[1], F. Angrilli[2], G. Arnold[3], S. Atreya[4], K.H. Baines[5], G. Bellucci[1], B. Bezard[13], F. Billebaud[9], D. Biondi[1], M.I. Blecka[7], L. Colangeli[16], L. Comolli[20], D. Crisp[15], M.D'Amore[1], T. Encrenaz[9], A. Ekonomov[6], F. Esposito[16], C. Fiorenza[1], S. Fonti[11], M. Giuranna[1], D. Grassi[1], B. Grieger[12], G. Hansen[19], J. Helbert[3], H. Hirsch[3], N. Ignatiev[6], A. Jurewicz[7], I. Khatuntsev[6], S. Lebonnois[13], E. Lellouch[9], A. Mattana[1], A. Maturilli[1], E. Mencarelli[1], M. Michalska[7], J. Lopez Moreno[10], V. Moroz[6+], B. Moshkin[6], F. Nespoli[1], F. Nuccilli[1], P. Orleanski[7], E. Palomba[16], G. Piccioni[8], M. Rataj[17], G. Rinaldi[1], M. Rossi[1], B. Saggin[20], D. Stam[14], M. Roos Serote[21], D. Titov[6], G. Visconti[17] & L. Zasova[6]

[1]*Istituto di Fisica dello Spazio Interplanetario IFSI INAF, Via del Fosso del, Cavaliere 100, I-00133 Rome, Italy*
Email: formisan@nike.ifsi.rm.cnr.it
[2]*Universita' di Padova, Dipartimento Ingegneria Meccanica, Via Venezia 1, I-35131 Padova, Italy*
[3]*Deutsches Zentrum für Luft- und Raumfahrt e.V. (DLR) Optische Informationssysteme, Rutherfordstrasse 2, D-12439 Berlin, Germany*
[4]*College of Engineering, The University of Michigan, Space Research Building, 2455 Hayward Street, Ann Arbor, MI 43109-2143, USA*
[5]*Jet Propulsion Laboratory, MS 133-601, 4800 Oak Grove Drive, Pasadena, CA 91011, USA*
[6]*Space Research Institute (IKI), Profsojuznaja 34/32,117310 Moscow, Russia*
[7]*Space Research Centre of Polish Academy of Sciences (SRC PAS), Bartycka 13A, 00716 Warsaw, Poland*
[8]*Istituto Astrofisica Spaziale IASF INAF, Reparto di Planetologia, Via del Fosso del Cavaliere 100, I-00133 Rome, Italy*
[9]*Observatoire de Paris Meudon, Department de Recherch Spatiale (DESPA), Place J. Janssen 5, F-92195 Meudon, France*
[10]*Istituto de Astrofisica de Andalusia CSIC, p.o.b. 3004, E-13030 Granada, Spain*
[11]*Universita' degli Studi di Lecce, Dipartimento di Fisica, Via Arnesano, I-73100 Lecce, Italy*
[12]*Max-Planck-Institute for Aeronomy, Max-Planck-Str. 2, D-37191 Katlenburg-Lindau, Germany*
[13]*LESIA, Observatoire de Paris, section de Meudon, Bât. 13, pièce 111, F-92195 Meudon cedex, France*
[14]*Astronomical Institute 'Anton Pannekoek', University of Amsterdam, Kruislaan 403, 1093 SJ Amsterdam, The Netherlands*
[15]*Jet Propulsion Laboratory, Earth and Space Sciences Division, Calfornia Institute of Technology, M/S 241-105, 4800 Oak Grove Drive, Pasadena, CA 91109-3099, USA*
[16]*Osservatorio Astronomico di Capodimonte (OAC), Via Moiariello 16, I-30131 Napoli, Italy*
[17]*Department of Physics, University of L'Aquila, Via Vetoio, I-67010 L'Aquila, Italy*
[18]*Laboratoire de Meteorologie Dynamique, Jussieu, Box 99, F-75252 Paris cedex 05, France*
[19]*Dept. of Earth and Space Sciences, Box 351310, University of Washington, Seattle, WA 93195-1310, USA*
[20]*Politecnico di Milano, Polo di Lecco,Via Marco D'Oggiono 13/A, I-23900 Lecco, Italy*
[21]*Observatorio Astronomico de Lisboa, Centro de Astronomia e Astrofisica da Universidade de Lisboa, Tapada da Ajuda, 1349-013 Lisboa, Portugal*

The Planetary Fourier Spectrometer (PFS) is an infrared spectrometer optimised for atmospheric studies, with a short-wavelength (SW) channel covering the spectral range 1800–11400 cm^{-1} (0.9–5.5 µm) and a long-wavelength (LW) channel covering 250–1800 cm^{-1} (5.5–45 µm). Both channels have a uniform spectral resolution of 1.3 cm^{-1}. It is the first Fourier spectrometer at Venus covering the 1–5 µm range. The SW field of view is about 1.6º FWHM, and 2.8º FWHM for the LW, which corresponds to spatial resolutions of 7 km and 12 km, respectively, when Venus is observed from a height of 250 km. PFS can provide unique data for improving our knowledge not only of the atmosphere properties but also the surface properties (temperature) and surface-atmosphere interaction (volcanic activity).

The SW channel uses a PbSe detector cooled to 200–220K, while the LW channel is based on a pyroelectric ($LiTaO_3$) detector working at room temperature. The intensity of the interferogram is measured at every 112 nm displacement of the mirrors (corresponding to 450 nm optical path difference), by using a laser diode monochromatic light interferogram (a sine wave), whose zero crossings control the double pendulum motion. PFS works primarily around the pericentre of the orbit, only occasionally observing Venus from large distances. Each measurement takes 4 s, with a repetition time of 11.5 s. By working for about 1.5 h around pericentre, a total of 460 measurements per orbit can be acquired, plus 60 for calibrations. PFS can take measurements at all local times, facilitating the retrieval of surface temperatures and atmospheric vertical temperature profiles on both the day and night sides.

PFS can measure a host of atmospheric and surface phenomena, including: the thermal surface flux at several wavelengths near 1 µm, with concurrent constraints on surface temperature and emissivity (indicative of composition); the abundances of several highly-diagnostic trace molecular species; atmospheric temperatures from 65 km to 90 km altitude; cloud opacities and cloud-tracked winds in the lower-level cloud layers near 50 km altitude; cloud-top pressures of the uppermost haze/cloud region near 70–80 km altitude; oxygen airglow near the 100 km level. Repeated observations during the 500-day nominal mission would yield an increased understanding of meteorological, dynamical, photochemical and thermo-chemical processes in the atmosphere. Additionally, PFS could search for and characterise current volcanic activity through spatial and temporal anomalies in the surface thermal flux and the abundances of volcanic trace species in the lower atmosphere. Measurement of the 15 µm CO_2 band is very important. Its profile gives, via a complex temperature profile-retrieval technique, the vertical pressure-temperature relation, which is the basis of global atmospheric studies.

1. Scientific Objectives

1.1 Introduction

The interest in Venus stems from the similarities and differences with Earth. Venus is a little smaller and, although it is closer to Sun, it assimilates a little less solar flux owing to its higher bolometric albedo. Before space probes, the general similarity of the two planets lead to speculation that under the impenetrable clouds of Venus there was a planetary surface similar to the equatorial regions of Earth. However, the first radio astronomical observations at cm-wavelengths in 1956 showed a spectrum typical of thermal emission. Two hypotheses were proposed then to explain its nature: radiation from a hot surface or from the ionosphere. Radar observations were in better agreement with the first hypothesis. More evidence came from remote measurements by Mariner-2 during its 1962 flyby. The final confirmation came in 1967 when the Soviet Venera-4 made *in situ* measurements in the atmosphere: it found high temperature, high pressure and carbon dioxide in abundance.

In all, 15 Soviet and 7 US missions explored Venus from 1962 to 1999. The full history was briefly described and chronologically tabulated by Moroz et al.

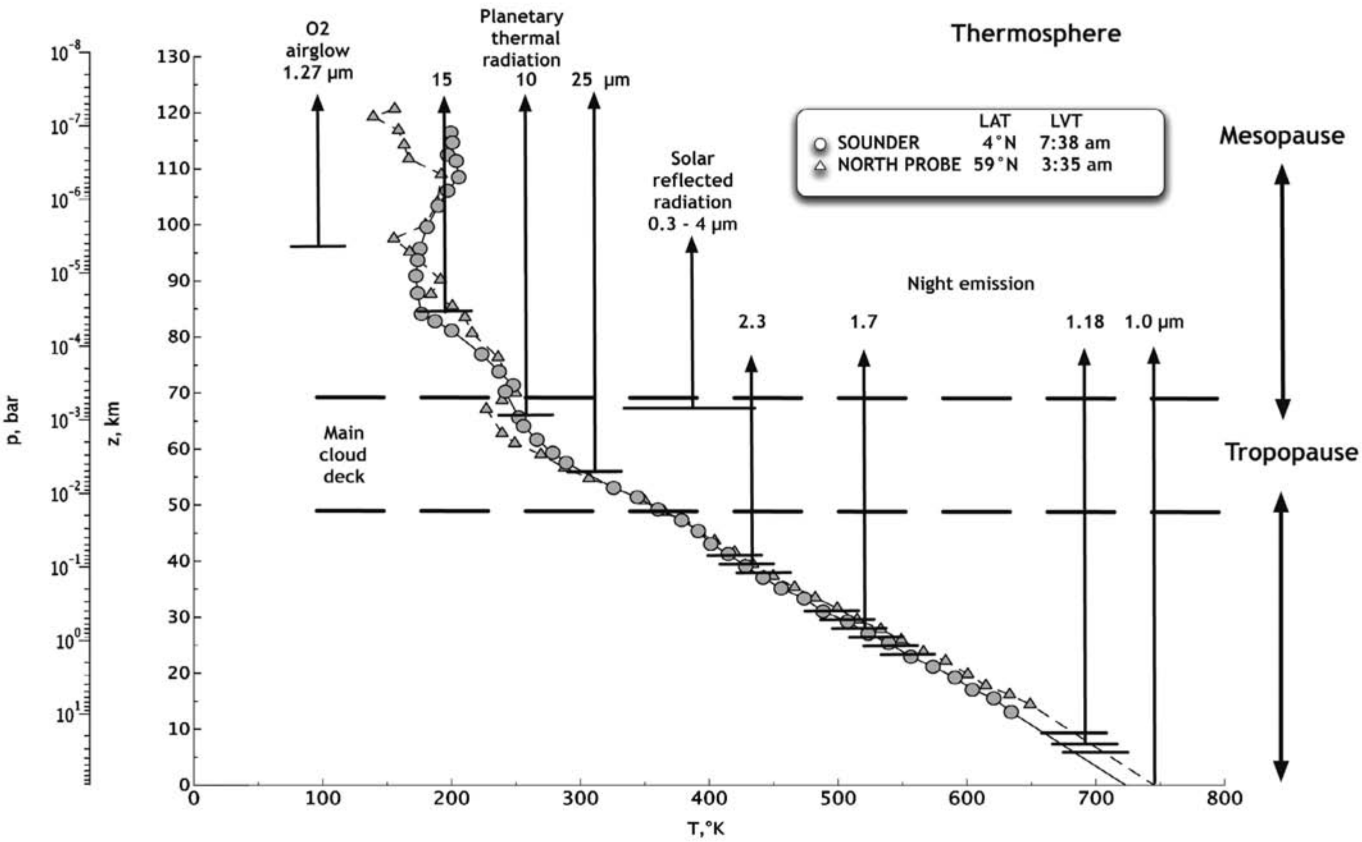

(2002) and Huntress et al. (2003). Galileo and Cassini were the most recent missions, using Venus for gravity-assist manoeuvres to reach Jupiter and Saturn, respectively. Some of their instruments returned data during the flybys. Until Venus Express, the last spacecraft dedicated to Venus exploration was Magellan (launched 1989).

The Planetary Fourier Spectrometer (PFS) is the key instrument for studying the middle and lower atmosphere. It was inherited from Mars Express with modifications required by the particular properties of the Venus atmosphere and its radiation. PFS has two spectral channels: one for the long wavelengths (LWC, 5.5–45 µm) and the other for the short (SWC, 0.9–5.5 µm). The spectral resolution is 1.3 cm^{-1} for both channels.

Fig. 1. The vertical structure of the atmosphere of Venus. Circles and triangles are measurements of the temperature profile from two of the four Pioneer probes (Seiff, 1983). They coincide within the troposphere, but there are differences in the mesosphere: inversions are observed at high latitudes and the low-latitude profile is relatively smooth. The approximate levels from which planetary radiation escapes to space are shown.

1.2 The atmosphere of Venus

The atmosphere of Venus is very dense; the ratio of its mass to the mass of the solid body is 10^{-4}, much more than for Earth ($2x10^{-7}$) and Mars ($5x10^{-9}$). Kuzmin & Marov, 1974; Moroz, 1981; Krasnopolsky, 1982; Hunten et al., 1983; Kliore et al., 1985; Barsukov et al., 1992; and Bougher et al., 1997 summarise our knowledge of the planet and its atmosphere. At the reference level (corresponding to the nominal surface radius of 6052 km), the temperature is 735K and the pressure is 92 bar. The most abundant atmospheric gas is CO_2. Its inventory is approximately the same as the total mass of carbonates on the Earth. The atmosphere also contains several percent of N_2. All other gases (see section 1.8) are minor constituents. The water abundance is very low on Venus; it is an extremely dry planet. There are interesting peculiarities in the content of some other volatiles, including noble gases.

The vertical structure of the atmosphere is presented in Fig. 1. Within the height range 0–55 km, the temperature lapse rate is nearly adiabatic, but between approximately 30 km and 50 km it is a little lower than adiabatic, resulting in the formation of two convective zones separated by a stable region. The principal feature of atmospheric general circulation is super-rotation, with typical wind speeds of 60–120 m/s. The whole planet is covered by cloud layers at heights of 49–70 km. However, a small but non-negligible part of the solar flux penetrates to the surface and heats the atmosphere via the greenhouse effect. Venus has no intrinsic magnetic field and the solar wind interacts directly with the ionosphere. The upper atmosphere is relatively hot on the dayside but very cold at night.

However, this picture is not completely clear. Very little is known about the atmosphere's general circulation below the clouds, its role in the planetary heat transfer, and the links between cloud structures and dynamics. Cloud particles in the upper clouds are mainly sulphuric acid in water solution; other condensates may exist, especially in the middle and lower clouds. The possible role of volcanic events in the atmospheric processes is also far from being understood.

At wavelengths shorter than approximately 3 µm, the clouds attenuate radiation by scattering rather than true absorption. By this mechanism, some SW thermal radiation from the deep hot atmospheric layers penetrates clouds through windows between the CO_2 bands and escapes to space. This radiation is negligibly small compared with the reflected solar radiation on the dayside, but it is visible on the nightside.

Figure 1 shows the approximate heights from which planetary thermal and reflected solar radiation leaves Venus at different wavelengths. This explains how observations in a wide spectral range remotely sounds the atmosphere over such a very wide range of heights. PFS, with its LW and SW channels, is an excellent tool for such sounding.

1.3 Historical background

Earth-based observations of Venus spectra in the thermal-IR have been made several times (Krasnopolsky, 1982), but strong terrestrial H_2O and CO_2 absorption masked the most interesting parts of these spectra. These Earth-based observations relate only to the disc-integrated radiation. Measurements from a Venus orbiter are, obviously, free of telluric absorptions and provide high spatial resolution. Before PFS, the only such measurements were made in 1983 by a Fourier spectrometer aboard Venera-15 (Moroz et al., 1986). Examples are shown in Fig. 2.

The spectral range of this instrument was 6–40 µm, with a spectral resolution of 5–7 cm^{-1}. The spatial resolution near pericentre was 200 km. Some 2000 high-quality spectra were obtained, but the instrument then failed after 2 months. The whole southern hemisphere and local times around noon and midnight were unexplored. These results clearly showed how effective an IR Fourier spectrometer can be for Venus exploration. Interpretation of the spectra continues (Moroz et al., 1986; Zasova et al., 1985, 1992, 1993, 1995, 1997, 1999, 2000, 2002; Titov, 1995; Titov et al., 1992; Ignatiev et al., 1999). Bands of H_2O and SO_2 in the thermal-IR spectra were observed for the first time using this experiment (section 2.8).

Another important experiment was the Orbiter Infrared Radiometer (OIR; Taylor et al., 1980) of Pioneer Venus Orbiter. It had only several filters but their selection provided a rough but representative sounding of the thermal and cloud structure. The important discovery was that outgoing thermal flux in the polar regions was greater than at the equator.

Dayside spectra were recorded earlier in Earth-based observations (Kuiper, 1962; Moroz, 1968; Connes et al., 1967, 1968, 1969) and aircraft (Kuiper & Forbes, 1967; Bjoraker et al., 1992). Observations by Connes et al. were made with extremely high resolution (0.1 cm^{-1} and later even better) by means of large telescopes and a sophisticated Fourier spectrometer. Measurements from

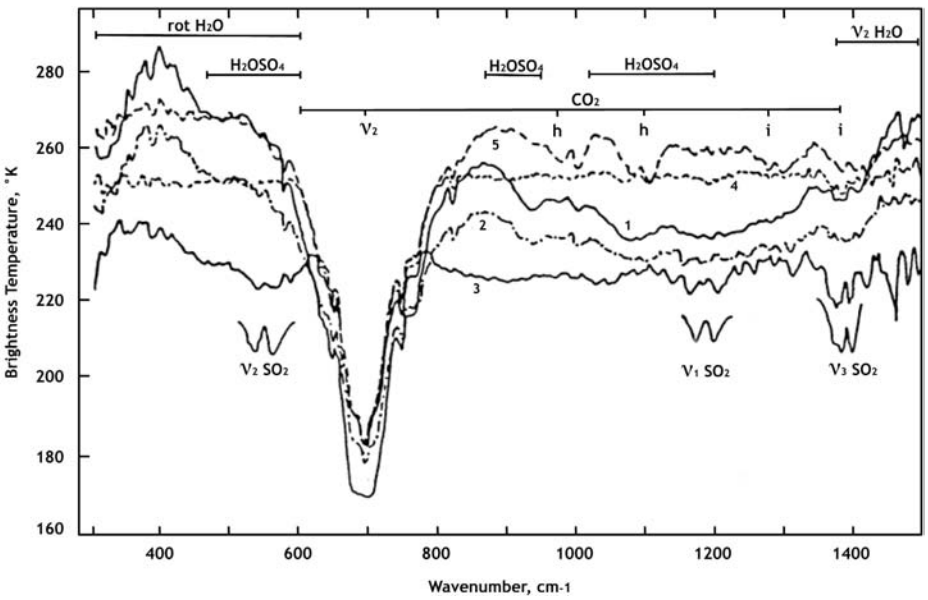

Fig. 2. Examples of spectra obtained by the Fourier spectrometer of Venera-15 in 1983. It covered approximately the same spectral range as PFS LWC but at lower spectral resolution. These are averaged (5–10 individual) spectra for different latitudinal zones: equatorial (1); mid-latitude, φ < 59 (2); high-latitude (60 < φ < 80), from the 'cold collar' (3); polar region, usually φ > 85 (4); hot dipole structure at high latitudes (5).

spacecraft have much lower resolving power but they are almost free from terrestrial CO_2 and H_2O absorptions and provide some spatial resolution.

Nightside spectra are even more interesting. They show weak thermal emissions escaping from the atmosphere below the clouds in windows between the CO_2 bands and provide information on abundances of the trace constituents in the lower atmosphere, plus their latitudinal, place-to-place and time variations. These weak night thermal emissions were discovered via Earth-based observations (Allen & Crawford, 1984), and observed later with high spectral resolution. No equivalent observations have been made from an orbiter, but some important measurements were made by the Galileo and Cassini spacecraft during their brief Venus flybys (Carlson et al., 1993a, b; Baines et al. 2000). The thermal radiation from the surface dominates the 1 µm night emission (Carlson et al., 1993a, b; Lecaucheux et al., 1993; Meadows & Crisp, 1996; Baines et.al., 2000).

There is also an interesting near-IR emission from the upper atmosphere: O_2 $^1\Delta$ airglow at 1.27 µm (Connes et al., 1979), observed both on the night and day sides. Its source is the recombination of O atoms produced on the dayside, mostly at 100–120 km. They are transported by global circulation to the nightside.

1.4 PFS goals

The Venus Express mission is focused on global investigation of the atmosphere and surface. PFS was designed (Tables 1 & 2) to provide fundamental new data on the characteristics of the climate and atmosphere important for studying important basic problems:

PFS LW channel

— long-term global 3-D measurements of the temperature field within the 55–100 km altitude range;
— subsequent determination of zonal and meridional components of the wind in the altitude range 55–100 km;
— monitoring of the upper cloud structure and composition;
— measurements of the abundances of SO_2 and H_2O at 60–75 km altitude;
— measurements of the outgoing thermal spectral fluxes (radiative balance);
— investigation of the thermal tides and periodicities in the temperature and

Table 1. PFS scientific objectives.

Atmospheric studies: global long-term monitoring of the 3-D temperature field in the lower atmosphere (from the clouds up to 90–100 km); measurements of the minor-constituent variations (water vapour and SO_2); search for possible other small components of the atmosphere; new determination of the D/H ratio; study of the optical properties of the atmospheric aerosols: dust clouds ice clouds hazes; determination of the size distribution and chemical composition; investigation of radiance balance of the atmosphere and the influence of aerosols on energetics of the atmosphere; study of global circulation, mesoscale dynamics and wave phoenomena.

Surface studies: surface-atmosphere exchange processes.

Table 2. PFS characteristics.

	SW	*LW*
Spectral range, μm	0.9 – 5.5	5.5 – 45
Spectral range, cm^{-1}	1800 – 11400	220 – 1800
Spectral resolution, cm^{-1}	1.3	1.3
FOV, rad	0.030	0.070
NEB, W cm^{-2} sr^{-1}	2×10^{-10}	3×10^{-8}
Measurement cycle, s	11.5	11.5
Detector type	photovoltaic	pyroelectric
Material	PbSe	$LiTaO_3$
NEP, W $Hz^{-0.5}$	3×10^{-13}	1.5×10^{-10}
Shape/size, mm	square, 0.7 x 0.7	round, >1.4
Temperature, K	200 – 220	290
Interferometer type	double pendulum	
Reflecting elements	cubic corner reflectors	
Beamsplitter	CaF_2	CsI
Max. optical path difference, mm	±5	±5
Time for motion, s	4	4
Reference source	laser diode	
Interferogram	two-sided	
Sampling number	22500	4500
Sampling step, nm	608	2432
Dynamical range	$\pm 2^{15}$	

zonal wind fields, in the upper clouds and possibly in the abundance of minor compounds.

PFS SW channel – dayside observations

— optical properties of the upper clouds from observations at different zenith and phase angles;
— mixing ratio of minor compounds (H_2O, SO_2, CO, HCl, HF) in the atmosphere above the clouds and near the cloud tops.

PFS SW channel – nightside observations

— study of the atmospheric composition (CO, COS, H_2O, SO_2, HCl) below the clouds;
— study of the cloud opacity and its variations;

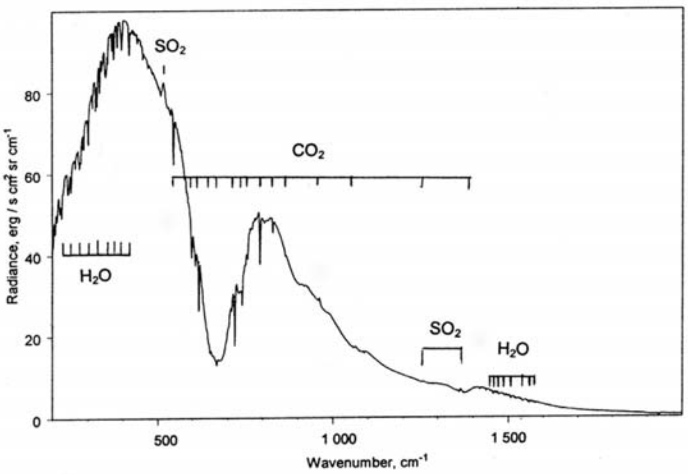

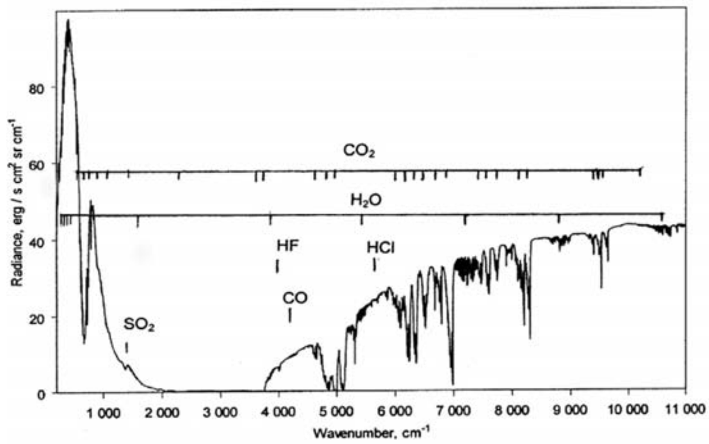

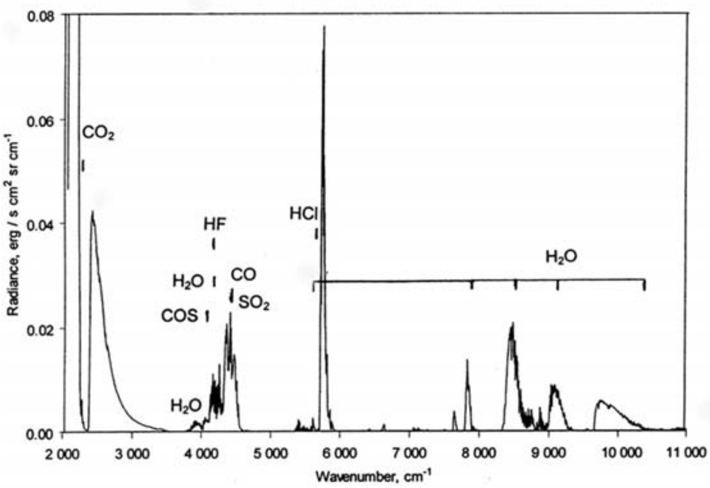

Fig. 3 (top left). Venus PFS LWC synthetic spectrum. It is almost the same on the day and nightside of the planet. If presented in terms of brightness temperature, the spectrum would be similar to that measured by Venera-15 (Fig. 2) but with about three times better spectral resolution.

Fig. 4 (top right). PFS synthetic spectrum for the dayside. The SWC range starts at 2000 cm^{-1} (5 μm).

Fig. 5 (left). Venus PFS SWC synthetic spectrum for the nightside of the planet.

- measurements of the temperature gradient at 0–10 km and the surface temperature;
- search for volcanic activity;
- thermal mapping of the surface in the 1 μm windows region;
- day and night monitoring of the airglow emission of the O_2 $^1\Delta$ ro-vibrational band at 1.27 μm.

Figures 3–5 present synthetic spectra of Venus in the PFS range. The spectrum of outgoing radiation (as for all planets) consists of two main parts: the reflected solar radiation and planetary thermal radiation. The boundary between them is near 2500 cm^{-1} (4 μm) for the dayside. All the pronounced spectral features are CO_2 bands; there are many other spectral features that belong to minor constituents such as CO and H_2O (see section 1.8) and can be used to estimate their abundances at different altitudes.

The shape of the LWC spectra is governed by the following factors:

- temperature profile;
- aerosol vertical profile, which defines the level of formation of radiation outside of the gaseous absorption bands;
- vertical profile and mixing ratios of the absorbing gases, including the CO_2 main constituent and the two H_2O and SO_2 minor constituents.

The most pronounced CO_2 spectral feature is the 667 cm^{-1} (15 µm) fundamental band. Other CO_2 features of special interest are the 961 cm^{-1} and 1064 cm^{-1} hot bands, and the 1259 cm^{-1} and 1366 cm^{-1} isotopic ($^{12}C^{16}O^{18}O$) bands. H_2O is visible in two parts of the LW channel spectrum: the 280–475 cm^{-1} rotational band, and the 1590 cm^{-1} (6.3 µm) roto-vibrational fundamental band. There are three bands of SO_2: ν_2 (519 cm^{-1}), ν_1 (1150 cm^{-1}) and ν_3 (1360 cm^{-1}). Some features belong to liquid sulphuric acid: 450, 580, 900, 1150 cm^{-1} (the 580 cm^{-1} feature is in the wing of the 667 cm^{-1} CO_2 band).

The shape of the SWC spectra of the dayside is governed by:

— multiple scattering of the solar radiation by particle clouds dominating above approximately >4000 cm^{-1};
— true absorption of the solar radiation by liquid sulphuric acid in cloud particles dominating below < 4000 cm^{-1};
— abundances of absorbing gases (CO_2, H_2O, CO, HCl, HF) within and above the upper clouds.

CO_2 features dominate everywhere. H_2O and CO bands are much weaker, but clearly visible. HCl and HF are extremely weak.

The shape of the SWC spectra of the nightside is governed by the following factors:

— temperature profile;
— vertical profile and mixing ratios of the absorbing gases, including the CO_2 main constituent and several minor: H_2O, SO_2, CO, COS, HCl, HF. Spectral features of the minor constituents are observable in windows between much stronger CO_2 bands;
— attenuation of radiation by clouds (for ν > 3500 cm^{-1});
— thermal radiation of clouds (for ν < 3500 cm^{-1});
— thermal radiation of surface (near 10 000 cm^{-1}).

The fundamental ν_3 CO_2 band near 2349 cm^{-1} is observable both in night and dayside spectra but in the latter case its formation is more complicated owing to superposition of the thermal and solar scattering radiation.

A more detailed discussion of the PFS scientific goals is provided in sections 1.5–1.12.

1.5 Temperature/aerosol retrieval

The atmosphere's thermal radiation exits to space from altitudes with optical depth $\tau = 1$ for a given wavenumber. Examples of spectral dependence of the altitude corresponding to $\tau = 1$ in the atmosphere of Venus are shown in Fig. 6. Both gas and aerosol particles contribute to the extinction coefficient at all wavelengths, but their relative role is different in different parts of spectrum. For example, only gaseous absorption is important in the central part of the strong 667 cm^{-1} CO_2 band. It is almost negligible far beyond this band, where the aerosol is responsible for the continuum extinction.

The general shape of this wide 667 cm^{-1} feature depends on the temperature profile in the mesosphere. So the local temperature profiles are retrievable from precise measurements of the spectrum inside the 15 µm CO_2 band. There is another strong CO_2 feature, which in principle may be used for temperature retrieval, namely the 2349 cm^{-1} band (see Figs. 4 & 5), In practice, however, this latter feature is not used, because of the lower radiance level and superposition with the solar scattered radiation on the dayside of the planet.

A set of weighting functions (gas + aerosol) for temperature retrieval for the low-latitude case (similar to curve 1 in Fig. 6) is presented in Fig. 7. For this case, a reliable temperature retrieval may be obtained in the altitude range 58–95 km. PFS spectral resolution was projected to be 1–2 cm^{-1}. The most important

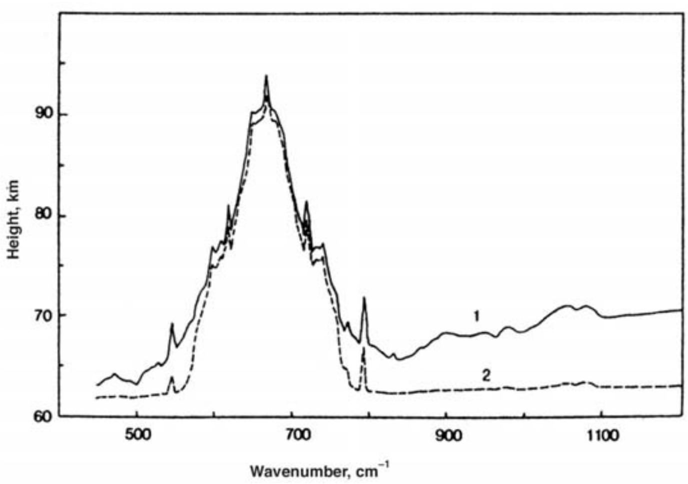

Fig. 6. Altitudes of the maximum of weighting functions (approximate τ = 1 level) versus wavenumber for two of the spectral groups shown in Fig. 2. Solid curve (1) is for group 2; dashed curve (2) is for group 3. For the low-latitude spectrum (curve 1), radiation in the wings of the 15 µm band (ν < 580 cm^{-1} and ν > 770 cm^{-1}) originates in the upper clouds.

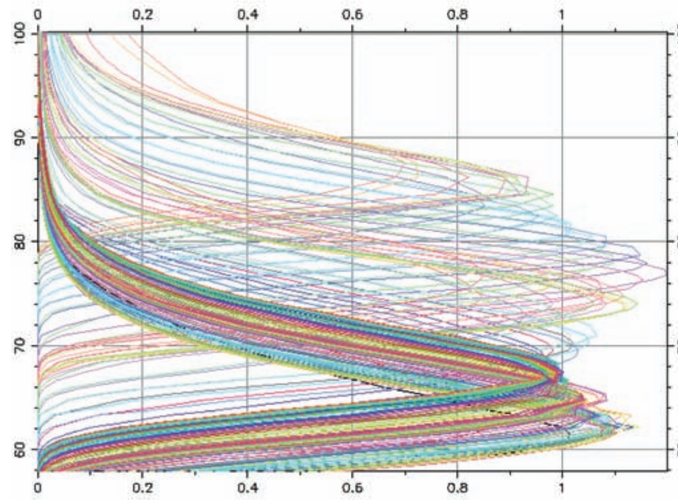

Fig. 7. Set of weighting functions (low-latitude case, curve 2, Fig. 6) used for temperature retrieval from Venera-15 data. Spectral resolution is about 7 cm^{-1} (Venera-15).

advantage of higher resolution for temperature retrieval is the possibility of higher accuracy of the temperature profiles at the levels around 100 km.

Temperature and aerosol vertical profiles should be retrieved in a self-consistent way from the same spectrum. The extinction cross-section of sulphuric acid particle in the thermal-IR spectral range may vary by a factor of 30, depending on particle size. The spectral regions where maximum and minimum of extinction coefficient occur are free from gas absorption and may be used for aerosol retrieval. For PFS, the minor constituents (such as SO_2 and H_2O) could also be included in the self-consistent procedure.

Temperature retrieval from the IR spectrum is the inverse problem for the transfer equation. For planetary atmospheres, two classes of methods are most frequently used: the Chahine relaxation method and its modifications, and statistical regularisation. Both were used as first steps towards temperature retrieval (using the approximation of a pure gaseous atmosphere) from Venera-15 data. However, it was later found that the relaxation method modification used (Twomay et al., 1977) works more effectively for self-consistent temperature and aerosol retrieval. A description of the relaxation method for self-consistent temperature and aerosol retrieval can be found in Zasova et al. (1999). The Tikhonov regularisation method (Tikhonov et al., 1990) may be also used in principle for solving the inverse problem.

1.6 Temperature in the middle atmosphere

The visible disc of Venus is highly inhomogeneous in the thermal-IR: the contrasts at high latitudes are up to 300%. These variations are caused by both temperature variations and variations in the upper clouds. Temperature profiles at low latitudes show inversion near 85–95 km; the shape of the inversion and its position depend on local time. The most pronounced inversion is observed in the 'cold collar' (60–80º). At higher latitudes (in polar regions), the temperature inversion is found at lower levels: around 58 km . The hot dipole differs from the surrounding near-polar region by higher temperatures at 55–60 km altitude and, practically, absence of the inversion. Several examples of the temperature profiles retrieved from Venera-15 data are shown in Figs. 8 & 9.

An example of the global average temperature profile field from Venera-15 is

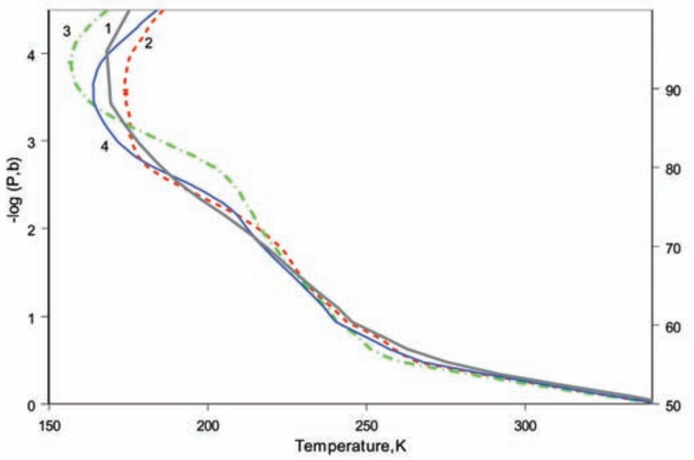

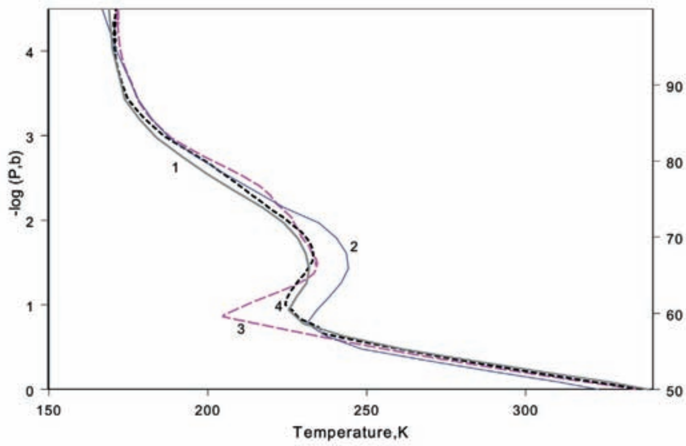

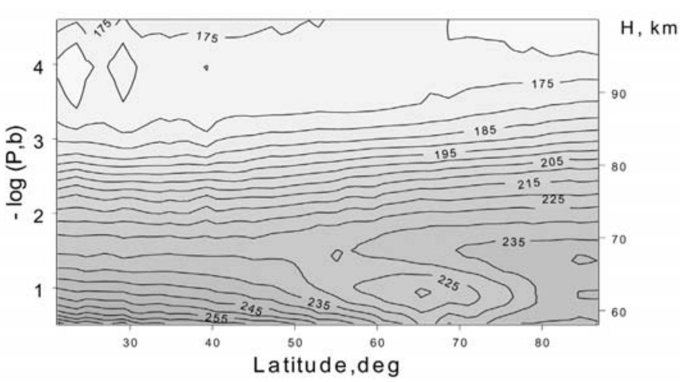

Fig. 8 (top left). Variability of the temperature profile at low latitudes in comparison with averaged model VIRA temperature profile. 1: VIRA 30, IR Venera-15. 2: $\phi < 35°$, L_S = 20–90º. 3: $\phi < 35°$, L_S = 270–310º. 4: $-10 < \phi < +10°$, L_S = 75º.

Fig. 9 (top right). The averaged IR Venera-15 profiles for the coldest part of the cold collar (3) and the warm areas at the cold collar latitudes (4) compared with the model VIRA 60º (1) and VIRA 75º temperature.

Fig. 10 (left). Global averaged temperature field obtained from the Venera-15 IR spectrometry data.

shown in Fig. 10. PFS will improve this result by adding better coverage in space and local time. Higher spectral resolution would help to obtain more accurate temperature profiles, especially at high levels in the atmosphere

1.7 Clouds and hazes

It is known that Venus' main cloud deck has an overall thickness of ~20 km and consists of three main regions: upper clouds, middle, and lower clouds (Moroz, 1981; Esposito et al., 1983). The optically thin upper haze is located above the clouds. The main properties of the upper clouds and haze derived from Venera-15 IR measurements were studied by Zasova et al. (1993, 1996), Zasova & Moroz (1992) and Zasova (1995). Two key parameters characterise this part of the cloud deck: the altitude of the cloud upper boundary (optical depth $\tau \sim 1$) and the aerosol scale height above it. A summary of estimates of these values is presented in Table 3. For latitudes below ~55º, the transition from clouds to haze is smooth, and aerosols are present up to 80–90 km. For higher latitudes, the upper boundary of clouds is mostly much sharper.

Upper clouds at latitudes >55º show an interesting variety of horizontal structure: cold collar, polar region and warm dipole. The cold collar is a low-temperature asymmetrical belt encircling the planet at about latitude 70º. A warmer polar region occupies higher latitudes. The most significant peculiarity of cloud structure at high altitudes is a dramatic dipole of two warm spots, marking a corresponding lowering of upper clouds and rotating with a period of 2.7 days. This complex picture was discovered by the OIR instrument of Pioneer Venus Orbiter. The Fourier spectrometer on Venera-15 showed that hot CO_2 spectral bands (near 10 μm) are much stronger there than anywhere else.

The size distribution of cloud particles has been measured by several *in situ*

Table 3. Altitude of Cloud Upper Boundary (Level of Optical Depth τ~1) and Aerosol Scale Height Above It.

Latitude zone (deg)	*Altitude of τ~1, km 365 cm^{-1}*	*1218 cm^{-1}*	*Aerosol scale height, km*
<55	57–59	67–69	3.5–4
55-75			
within cold collar	58–60	60–62	<1
outside cold collar	56–60	70–72	>4
75-85			
within hot dipole	56–58	59–64	1–1.5
outside hot dipole	61–63	63–64	<1
>85	62–64	62–64	0.5

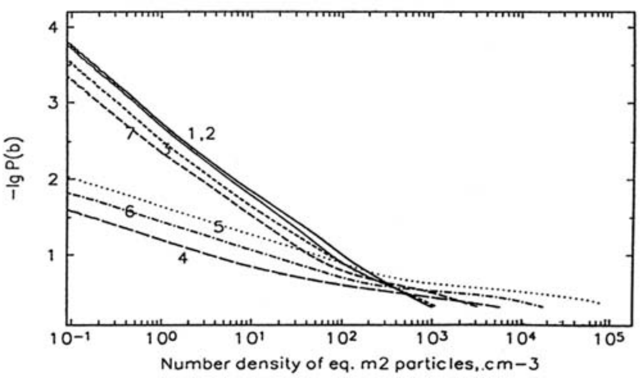

Fig. 11. Equivalent particle number density for various local conditions. 1: latitudes ϕ < 35ºN, 0 < L_S < 90º (day). 2: for same latitudes but 270 < L_S < 320º (night). 3: for ϕ from 10ºS to 10ºN, L_S = 320º. 4: for the 'cold collar' (60 < ϕ < 80º). 5: for north polar region (ϕ > 85º). 6: for the 'hot dipole' (75 < ϕ < 85º). 7: for warm areas at the same latitudes as the cold collar.

experiments. It is multimodal, although there are some controversies in mode definition. Description by three modes is the most common: mode 1 (0.5 µm mean diameter), mode 2 (2–3 µm) and mode 3 (largest particles). Mode 2 dominates in the upper clouds.

An important message from Venera-15 Fourier spectrometer observations is that, at all latitudes, the sulphuric acid water solution is the main constituent of aerosols in the upper clouds and haze. Only for wavenumbers < 400 cm^{-1} were some discrepancies found, but their nature is not clear. They may be due to errors in published values of H_2SO_4 and H_2O optical constants, simplifications in adopted size distribution or an indication of the presence of particles with other chemical compositions.

PFS was designed to provide important progress in cloud studies by combining three observation modes: LWC (as Venera 15), SWC night (as Galileo) and SWC day (for the first time). SWC day measurements of CO_2 bands would give direct and reliable estimates of the altitude of the boundary of the upper clouds at high latitudes where aerosol scale height is small. At latitudes below 55º, interpretation would be more complicated. Here, the scattering coefficient in the upper clouds may be obtained from CO_2 daily SW band measurements using aerosol scale height taken from the thermal-IR.

1.8 Minor constituents

Minor constituents in the atmosphere have been measured by different methods and different platforms: spectroscopy from Earth, orbiters, flyby spacecraft and by chemical analysers, gas chromatographs and mass spectrometers aboard probes. Some Venera landers also carried small optical spectrometers. Reviews of the results were presented by Moroz (1981), von Zahn et al. (1983, 1985) and

Table 4. Minor constituents identified in the atmosphere of Venus (excluding noble gases).

Molecule	*Mixing ratio, ppm*	*Altitude, km*	*References*	*Comments*
H_2O	30–40	0–40	1–4	NIR night emissions and optical spectrometry on Venera 11,13,14
	2–30	58–62	5	Thermal IR, FS on Venera 15
D/H	120±40 terr	65–70	6	Dayside reflection spectrum
SO_2	130±35	<42	7	Venera 12 Chromatograph
	120±20	42	8	Vega 1, 2, UV on probe
	30–40	22	8	Vega 1, 2, UV on probe
	130±40	35–45	9	Night emissions
	1×10^{-6}–1.0	69	10	Thermal IR, FS of Venera 15
CO	23±7	30	1, 9	Night emissions
	29±7	40	1, 9	
			11	Dayside reflection spectrum
COS	0.35±0.1	30	1, 9	Night emissions
HCl	0.5±0.15	15–30	9	Night emissions
		65–70	12	Dayside reflection spectrum
HF	0.005±0.002	30–40	9	Night emissions
		65–70	12	Dayside reflection spectrum
H_2SO_4	11–20	40	13	13 cm radio occultations (gas phase below clouds; condensed phase in upper clouds shows a broad continuum and diffuse band absorptions)

References: (1) Pollack et al.,1993, (2) deBergh et al., 1995, (3) Meadows & Crisp, 1996, (4) Ignatiev et al., 1997, (5) Ignatiev et al., 1999, (6) deBergh et al., 1991, (7) Gelman et al., 1979, (8) Bertaux et al., 1996, (9) Bezard et al., 1993, (10) Zasova et al., 1993, (11) Connes et al., 1968, (12) Connes et al., 1967, (13) Jenkins & Steffes, 1991,1994.

Esposito et al. (1997). Information about the minor constituents identified and measured with IR spectrometers is presented in Table 4. All would be observed by PFS; the positions of the corresponding spectral bands are shown in Figs. 3–5.

Table 4 starts with H_2O and SO_2. These two molecules are interesting for two reasons: both are greenhouse gases, and they are involved in cloud chemistry. PFS could measure them within the upper clouds (LWC and SWC) as well as in lower atmosphere (SWC, night emissions). Both show strong variability (with altitude and latitude), an important target for PFS observations.

CO in the lower atmosphere demonstrates no or little altitude variability, but some variations with latitude have been observed and interpreted as dynamical tracers (Taylor et al., 1997).

COS should be involved in sulphur chemistry. It has been observed from Earth only with very high resolution in night emission. There is no information about latitudinal dependence. It would be a difficult task to distinguish it with PFS.

The HCl and HF mixing ratios are very low, so their observation must also be difficult. These gases may be related to volcanic eruptions, so their place-to-place variations (if they exist) may say something about volcanoes on Venus.

Estimates of upper limits for gases that have not been identified in the atmosphere are published in several sources (Moroz, 1981; von Zahn et al., 1983; von Zahn & Moroz, 1985). These gases include O_3, C_3O_2, CH_4, C_2H_2, C_2H_4, H_2S, N_2O, NO_2 and many others that have absorption features in the PFS range. Corresponding upper limits are low (< 10^{-3} ppm) but PFS could have provided in many cases even lower new values. Some of the upper limits will be replaced by positive identifications through PFS observations. These studies will not be limited to the dayside of Venus, but will possibly be extended to the nightside.

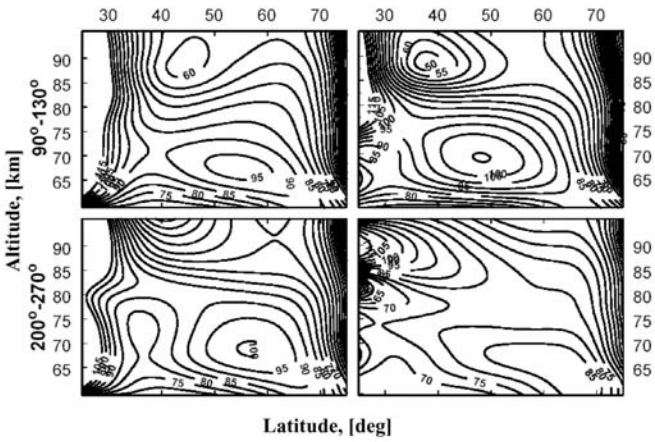

Fig. 12. The thermal wind field obtained from the averaged temperature field in the longitude ranges 20–90º (morning dayside), 90–130º (post-midnight sector), 200–270º (evening nightside), and 270–310º (afternoon). For more details, see Zasova et al. (2000).

PFS exploits seven atmospheric windows between 0.85 µm and 2.5 µm on the nightside to sample the lower atmosphere and surface. Within the 1.7 µm and 2.3 µm windows, the spectra can be analysed to infer the abundances of several key trace gases, including H_2O, SO_2, CO, OCS and HCl at levels between the base of the m ain cloud (~47 km) and the surface (Crisp et al., 1989, 1991a; Bezard et al., 1990; Grinspoon, 1993; Pollack et al., 1993). The intensity at wavelengths beyond the gas absorption bands provides information about the opacity and vertical distribution of the clouds. The spatial patterns mapped by PFS using spacecraft scanning techniques give the motions of cloud layers at 50 km and 57 km altitude, which appear silhouetted against the warmer layers below. The radiation measured in five atmospheric windows between 0.8 µm and 1.2 µm originates primarily at the surface. Observations in these windows provide information about the surface temperature, surface emissivity and near-surface thermal structure (Meadows & Crisp, 1996). These windows were used during the flyby observations of the Galileo/Near-Infrared Mapping Spectrometer (NIMS; Carlson et al., 1991, 1993b) and the Cassini/Visible and Infrared Mapping Spectrometer (VIMS; Baines et al., 2000). More recently, such techniques to reveal surface emissivities were supported by theoretical work (Hashimoto & Imamura, 2001; Moroz, 2002; Hashimoto & Sugita, 2003). PFS was intended to obtain the first time-resolved global maps of the surface in these spectral windows.

1.9 Thermal winds

The atmosphere principally exhibits zonal super-rotation. Venus is a slowly rotating planet, so the dynamics of its atmosphere are determined by a cyclostrophic balance, in which the centrifugal force acting upon a unit mass is counterbalanced by the meridional component of the pressure gradient.

Venera-15 measurements allowed the 3-D zonal wind field to be defined for the first time, and found zonal wind dependence with local time. Venera-15's polar orbit meant that a wide range of latitudes was observed during a single session practically at the same local time, which allowed the data to be used without global averaging (Zasova et al. 1997, 2002).

To show the local time variation of the zonal wind velocity, the data, averaged over four quadrants (morning dayside, morning nightside, evening nightside and evening dayside) are given in Fig. 12. The correlation with the temperature in the cold collar is clearly seen: the lower the temperature, the higher the wind velocity. Maximal wind speed is observed on the morning dayside, where the minimal temperature is observed. Conversely, minimal speed occurs on the evening dayside, where the cold collar is less pronounced.

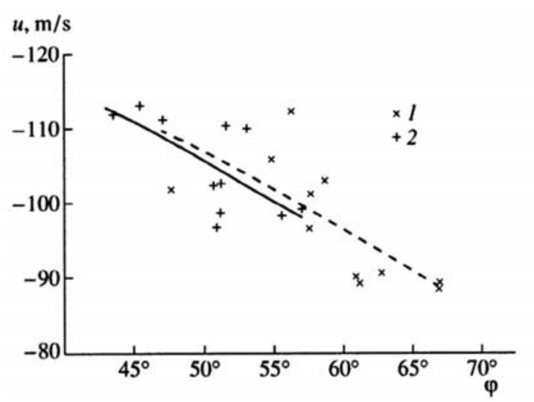

Fig. 13. Wind speed in the mid-latitude jet versus latitude. x: morning side, +: evening side.

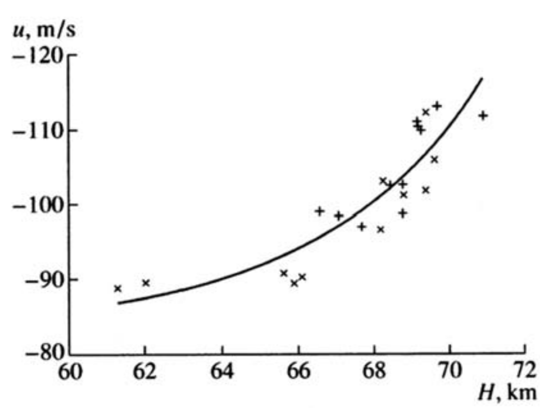

Fig. 14. As Fig. 13, but for wind speed versus altitude.

The mid-latitude jet changes its altitude and latitude with wind speed. The observed wind speed varies with latitude such that angular momentum is conserved (Fig. 13). It also correlates with altitude (Fig. 14). The wind speed in the jet is fitted by an exponential law with a scale height of about 4 km, which is not far from the value of atmospheric scale height. It is a factor in favour of flux conservation. The lowest position of the jet corresponds to its highest latitude and the lowest velocities; both are reached simultaneously in the afternoon.

PFS was designed to improve wind observations, providing better coverage in space and local time. Higher spectral resolution would help to obtain more accurate temperature profiles, especially at high levels in the atmosphere, and a more accurate wind field, for possibly both zonal and meridional components. Monitoring of the cloud features in the SW channel would provide information on wind speed in the cloud deck.

1.10 Thermal tides and solar-related structures

More than 70% of the solar energy absorbed by Venus is deposited in the middle atmosphere. The largest fraction is absorbed in the upper clouds above 58 km by an unknown UV absorber; the other significant sources of optical depth are the sulphuric acid aerosols, carbon dioxide, water vapour and sulphur dioxide. This unusual distribution of the absorbed energy is responsible for generation of the thermal tides, which play an important role in the support of the observed super-rotation of the atmosphere, the nature of which is not clearly understood. Propagation of the tides in the atmosphere is different for different harmonics and hence the levels of dissipation differ for different harmonics. Detailed investigation of the distribution of thermal tides is a key problem for modelling the super-rotation phenomena. Some results on the tide investigation, obtained from the Venera-15 data, are shown below. Temperature, clouds and zonal wind local time variations in the mid-latitude jet were investigated to search periodicity. Fourier deconvolution allowed five harmonics to be extracted: from zonal average to 1/4 day.

Venera-15 observations did not cover the whole day: the near-midday and midnight data are absent. However, the tidal maxima and minima are shifted from midday and midnight, which allowed them to be observed by Venera-15. The polar orbit of Venera-15 was also very favourable for observing solar-related structures. The amplitudes and phases of the tidal components depend on latitude and altitude in the atmosphere.

1.11 Radiative energy balance

Radiation plays an important role in various processes on the planets. It defines atmospheric temperature structure, controls photochemistry and induces the

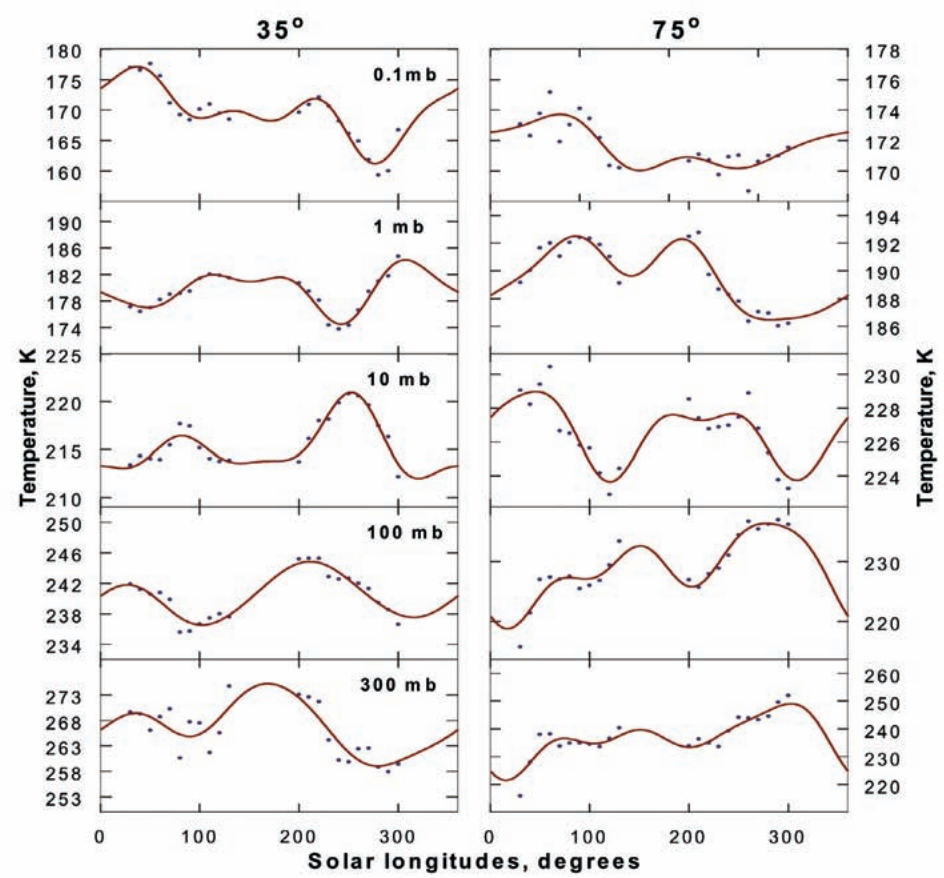

Fig. 15. An example of the temperature behaviour at isobaric levels (0.1, 1, 10, 100, 300 mbar) averaged over 10º of latitude and 10º of solar longitude for low (35º) and high (75º) latitudes. The fitting curves follow the Fourier expansion with the harmonics, conserving up to 1/4 Venusian days (wavenumber 4).

atmospheric motions. Venus offers examples of radiation-related processes that are unique in the Solar System. First, the planet holds the record for the greenhouse effect, which maintains the surface temperature of ~735K (Crisp & Titov, 1997, and references therein). Second, Venus has an unusual latitudinal distribution of outgoing thermal flux: receiving the solar energy at low latitudes, the planet emits a considerable portion of it to space from the poles (Taylor et al., 1980; Linkin et al., 1987). This implies a significant role for the atmospheric dynamics in heat transport.

Despite extensive Venus exploration in past decades, significant gaps remain in our knowledge of the radiation field outside and inside the atmosphere. The most important open questions involve:

— the global energy balance between the incoming and outgoing radiation;
— the distribution of heat sources in the atmosphere that drive the dynamics;
— the role of gases and aerosols and their variations in the greenhouse effect;
— the efficiency of the radiative energy escape from the lower atmosphere through the near-IR transparency windows (the 'leaking greenhouse').

PFS was designed to address these problems:

— the instrument will measure the spectrum of outgoing radiation over a broad range covering thermal and near-IR. Combined with the VIRTIS spectral measurements in the visible and UV, Venus Express will yield a full description of the radiation field escaping Venus.
— PFS will measure the spectrum of the near-IR emissions on the nightside, thus quantifying the efficiency of the 'leaking greenhouse.

— composition of the lower atmosphere derived from PFS spectroscopy in the near-IR windows will constrain the greenhouse models.
— the mesospheric temperature and cloud structure retrieved from the PFS measurements will be used for extensive modelling of the distribution of radiative heat sources in the mesosphere in order to understand the forces driving global circulation. Further insight into the atmospheric dynamics will be obtained by comparison of the 'thermal wind' field derived from PFS measurements and apparent cloud motions observed by the VIRTIS and VMC instruments of Venus Express.

1.12 The surface

The surface of Venus is dominated by plains with a large morphological diversity, including impact craters, young volcanic features and traces of lava fluids. There are also mountains up to 10 km elevation. The surface age is estimated at about 500 My. Soil composition is mainly different types of basalt.

The surface is so hot (~735K) that even at noon on the equator its thermal radiation in the 1 μm window is an appreciable part (about 10%) of the full surface brightness. The 1 μm thermal radiation from the surface penetrates the clouds. It was detected on the nightside from Earth (Meadows & Crisp, 1996) and by the Galileo (Carlson et al., 1993a) and Cassini (Baines et al., 2000) spacecraft. Clouds attenuate this radiation but add nothing to it owing to their low temperature.

An orbiter can use the 1 μm window to map the surface. However, there are three problems linked with the transfer and reflection of the surface thermal radiation by the clouds:

— clouds reflect part (about 80%) of the upwelling thermal radiation in the 1 μm window, and transmit about 20%. This value depends on the local optical depth of the clouds. So it would not be easy to distinguish between the variations of surface brightness and cloud optical depths. Imaging of the nightside in several (minimum two) windows could possibly solve this problem by separating the two contributions. The second window should be selected in the part of spectrum dominated by atmospheric radiation.
— multiple scattering of upwelling radiation within the clouds spreads the image. The size of the spot created by this spread must be roughly twice the height of the main cloud deck above the surface. This is about 100 km, so near-IR surface imaging from an orbiter cannot provide a spatial resolution better than that.
— multiple reflections between surface and clouds. It was shown (Moroz, 2002) that it leads to low sensitivity of measured brightness to emissivity of the surface.

Finally, measurements of outgoing night emission at 1.02 μm can provide information about the horizontal variations of surface temperature but not emissivity. The temperature must vary from place to place owing to topography. The thermal gradient in the atmosphere is 7.5– 8K/km (Seiff et al.,1985; Linkin et al., 1987; Meadows & Crisp, 1996). In this case, a height difference of 100 m leads to a 2% difference in the $B_P(T_S)$ value for 1.02 μm. So surface imaging in the 1 μm window can give information about topography.

Surface and near-surface thermal and compositional measurements by PFS were designed to help Venus Express reveal for the first time crucial geological, dynamical and chemical links between the hot, pressurised surface and the overlying chemically reactive atmosphere. In particular, PFS will observe the near-surface atmospheric lapse rate and its spatial/temporal variability, and the chemical, dynamical and thermal effects of active volcanism (if present) on the atmosphere and surface.

1.12.1 Surface atmospheric lapse rate

Direct measurement of temperature lapse rates in the planetary boundary layer (0–12 km) are limited to localised measurements by the Vega-2 lander (Linkin et al., 1987) and the Venera-8–10 landers (Avduevskiy et al., 1983). More recent ground-based near-IR spectral studies (Meadows & Crisp, 1996) suggest that the lapse rate may vary considerably over the planet. In particular, measurements of the Beta Regio region indicate that the lower atmosphere is remarkably subadiabatic, with a lapse rate of 7.5K/km, in contrast to the expected 8.3K/km adiabatic rate. Conversely, theoretical considerations (Dobrovolskis, 1993) indicate that the atmosphere could be statically unstable and turbulent in places, owing to the influence of topography on atmospheric winds and small yet significant variations in surface heating caused by variations in slope, surface emissivity/conductivity and latitude. Pettengill et al. (1996) noted that the critical altitude at which the Venus highlands show low radar emissivity increases by 1.5 km from the equator to high northern latitudes, perhaps reflecting a latitudinal variation in the atmospheric lapse rate. Measurements of the vertical lapse rate and/or horizontal and temporal gradients would directly address Pettengill's hypothesis, as well as enable evaluations of mechanical surface weathering owing to entrainment of particles in turbulent surface winds (Dobrovolskis, 1993).

Observations by NIMS (Carlson et al., 1991; Carlson et al., 1993b, c.f., Fig. 1, panel C), Cassini/VIMS (Baines et al., 2000) and ground-based observers (Lecacheux et al., 1981; Meadows et al., 1992; Meadows & Crisp, 1996) in the 0.85, 0.90, 1.01, 1.10 and 1.18 µm windows detected thermal emissions from the surface. Following Meadows & Crisp (1996), PFS will correlate 1 µm flux measurements with Magellan-derived surface topography to constrain thermal profiles from 0 km to ~12 km altitude. The degree of near-surface static stability will be ascertained by the thermal gradient measured on mountain slopes (Ishtar Terra in the northern polar region, Beta Regio at mid latitudes, Aphrodite at low latitudes). Temporal variations in surface flux will be used to discriminate the transient effects of dynamics from the thermal emissivity of surface materials.

PFS will produce greatly enhanced coverage and increased thermal accuracy compared to Earth-based measurements, which, owing to the Venus-Earth orbital resonance, are restricted to a small range of longitudes every 18 months. PFS surface temperature observations will be used to determine the lapse rate up to ~12 km altitude, while providing improved spatial resolution (~50–100 km over the north polar region, compared to the ~250 km from terrestrial observatories), and much more comprehensive spatial and temporal sampling and coverage.

1.12.2 Volcanism

Magellan crater counts indicate that the surface of Venus is geologically young (~500–1000 Myr). This, and the presence of a highly reactive sulphuric-acid cloud cover with a mean lifetime of 2 My, suggests the possibility of current volcanic activity. PFS will readily observe volcanic activity by its above-average thermal flux, enhanced gaseous absorptions and increased atmospheric scattering/ absorption from ejected dust plumes. Such data would be immensely useful in characterising the role that volcanism plays in climate change and stability and in assessing the character of interior processes within a dry planet. Chemical weathering of high-dielectric-constant surface material generated by volcanism, such as perovskite minerals, pyrite and pyrrhotite, may be observed as a spatially and temporally localised change in surface radiation. Laboratory studies under simulated Venusian conditions of iron sulphide chemical weathering have revealed that FeS_2 and Fe_7S_8 decompose over timescales of weeks to years. At high elevations, high-dielectric materials are ubiquitous at microwave wavelengths (Pettengill et al., 1988, 1992; Klose et al., 1992). PFS will globally map surface thermal emissions within the five surface-detection windows from 0.85 μm to 1.18 μm (Baines et al., 2000). These observations will be correlated with extant radar-determined surface emissivity and elevation maps to look for compositional differences among surface basalts such as the relative distribution of silicates and sulphides, as demonstrated theoretically by Hashimoto & Sugita (2003), and more exotic volcanic deposits and high-elevation materials.

Any temporal/spatial change in the H_2O and HDO abundances associated with volcanic activity would help to clarify the long-term evolution of both the atmosphere and the solid planet. As noted earlier, the observed atmospheric D/H ratio is ~150 times greater than the telluric ratio (deBergh et al., 1991; Donahue & Hodges 1993). PFS measurements of magmatic water and HDO released in a volcanic eruption would yield valuable insights into the evolution of the H_2O-poor atmosphere and the efficacy of present theories of global tectonics, insights into volcanic activity and constraints on the oxidation rate of the planet's crust.

1.13 Chemistry, evolution and the stability of the atmosphere

The evolution of the atmosphere of Venus has taken a different path than that of Mars owing to the runaway greenhouse effect. As a result, water is much less abundant and the D/H ratio is much greater than on Mars.

PFS will yield important constraints on the abundance of HDO, a key to understanding the evolutionary history of the atmosphere. Owing to a variety of suspected endogenic and exogenic processes – including the effects of cometary bombardments, the solar wind and the runaway greenhouse effect – the atmosphere today is vastly different from that at the planet's formation. The large ratio of deuterium to hydrogen in H_2O (some 150 times that found on Earth) attests to the loss of most of the water on Venus during its evolution. The mechanisms responsible for the higher D/H ratio are controversial and range from the loss of a primordial ocean to steady-state mechanisms, wherein H_2O supplied by cometary infall and volcanic outgassing is lost by atmospheric H_2 escape and oxidation of Fe-bearing crustal minerals (Grinspoon, 1993). The size of the initial water inventory is also quite uncertain, with estimates ranging between the equivalent of 5 m and 500 m of liquid water. The large uncertainty arises from a lack of precise measurements of the D/H ratio, as well as uncertainties in the current loss rate of H and O.

A particularly good diagnostic is the HDO/H_2O ratio and its variation with altitude. PFS was to make this measurement, using nadir views as well as limb scans and occultations. Measurements of H_2O and HDO acquired simultaneously by PFS will yield direct constraints on the D/H ratio at altitudes below ~100 km. A comparison of this result with that deduced from UV airglow measurements of the SPICAV instrument aboard Venus Express will help to determine the homopause level, and hence the eddy diffusion coefficient in a robust manner. In turn, the latter would place stringent constraints on photochemical models that are central to understanding the chemical cycles that regulate and maintain stable levels of the atmospheric species and the atmosphere as a whole and the atmospheric loss rates.

The long-term stability of the 90-bar CO_2 atmosphere is also still a mystery since CO_2 can be destroyed by photolysis ($\lambda \leq 0.250$ μm) on a relatively short time scale, and since the products (CO and O) do not combine to recycle CO_2. Indeed, all CO_2 in the atmosphere can be destroyed in 5 My. Whereas on Mars the hydroxyl radicals (OH) are believed to play a critical catalytic role in maintaining the stability of CO_2 there (by recycling CO and O or CO and O_2 (formed upon O+O recombination) into CO_2), this mechanism fails on Venus. This is due to the relatively small mixing ratio of water vapour and an efficient removal of the HO_x along with the depletion of O_2 in the process of formation of the hygroscopic sulphuric acid ($2\ SO_2 + 2\ H_2O + O_2 \rightarrow 2\ H_2SO_2$) in the Venusian atmosphere. It

Table 5. PFS Measurement Objectives and Uncertainties.

Measurement Objective		*Best Diagnostic Wavelength (µm)*	*Spatial Sampling at 5000 km Distance. Distance/Best Temporal Sampling*	*Measurement Precision**	*Accuracy*
Cloud Distribution and Winds				*m/s***	*m/s*
50 km altitude (night)		1.73, 2.30	136 km/1.5 h	4.5	4.5
57 km altitude (day)		1.72, 2.30	136 km/1.5 h	4.5	4.5
		0.95	136 km/1.5 h	4.5	4.5
Temperature Mapping				*K*	*K*
Surface (1–10 km)		0.85, 0.90,1.01, 1.10, 1.18	136 km/1.5 h	0.5	3
65 km		11.5	238 km/1.5 h	0.1	1.5
70 km		13.1, 4.56	136 km/1.5 h	0.1	1.5
75 km		13.5, 4.84	136 km/1.5 h	0.1	1.5
80 km		13.8	238 km/1.5 h	0.1	1.5
85 km		14.3	2.38 km/1.5 h	0.1	1.5
90 km		14.7	2.38 km/1.5 h	0.1	1.5
Surface Properties				%	%
Thermal emission/emissivity constraints		0.85, 0.90, 1.01, 1.10, 1.18	136 km/1.5 h	2	20
Airglow				%	%
O_2 ($^1\Delta$) near 100 km		1.27	136 km/1.5 h	5	10
Cloudtop Altitude/Pressure (τ = 1)				*km*	*km*
65 km		11.5/13.1	238 km/1.5 h	<0.1	0.2
70 km (day)		2.7	136 km/1.5 h	0.2	0.2
Atomic/Molecular Abundances				%	%
Species	*Altitude (km)*				
H_2O	0–12	1.10–1.18	136 km/1.5 h	5	20
	23	1.74	136 km/1.5 h	10	20
	33	2.40–2.43	136 km/1.5 h	4	20
HDO	33	2.38–2.46	136 km/1.5 h	20	50
	30	2.3	136 km/1.5 h	3	20
CO	42	2.33	136 km/1.5 h	3	20
OCS	30	2.425	136 km/1.5 h	7	20
	37	2.435	136 km/1.5 h	7	20
SO_2	39	2.46	136 km/1.5 h	9	20
HCl	39	1.74	136 km/1.5 h	15	30

*precision denotes the uncertainty in temporal or pixel-to-pixel spatial variations, and is driven by the S/N of the measurement. Accuracy denotes the uncertainty in absolute quantities, typically driven by uncertainties in the absolute calibration of the instruments and the modelling/analysis procedures used to derive such quantities. Precision/accuracy estimates based on Carlson et al. (1991) and Baines & Carlson (1991) for winds; Carlson et al. (1991) and Crisp et al. (1991a) for abundances and pressures, and Carlson et al. (1991) and Meadows & Crisp (1996) for temperatures.

**cloud-tracked wind precisions/accuracies determined from 24 h samples obtained at 10 000 km.

has been suggested that chlorine in the Venus atmosphere might play a catalytic role similar to that of OH in the Martian atmosphere (Yung & DeMore, 1982). If that is the case, models predict the presence of several critical chlorine compounds in the atmosphere of Venus, including ClCO, $ClCO_3$, ClOO, ClO, HCl and Cl_2. Note that chlorine would also participate in the sulphur chemistry, producing a number of species, the most abundant of which is expected to be sulphuryl chloride (SO_2Cl_2) at the ppm level.

PFS will be used to detect and measure the abundances of many diagnostic species, including several of these chlorine and sulphur species. PFS data will also be used to determine associated vertical mixing information. The results will be used in physico-photochemical-thermochemical models to understand the present state of chlorine, sulphur and water chemistry and to develop detailed models of the evolution, climatology and the stability of the atmosphere of Venus (Atreya, 1986; Wilson & Atreya, 2003).

1.13.1 Chemistry, composition and transport

PFS will be used to produce time-resolved global maps of the abundances of reactive species, to diagnose chemical and dynamical processes throughout the upper, middle and lower atmospheres. Venus' atmospheric chemistry involves complex and varied chemical cycles – H_2SO_4 cloud formation from H_2O and SO_2, CO generated by photochemistry, OCS and HCl produced by thermochemistry, and SO_2, H_2O and HCl in volcanic gases. All of these gases will be measured by PFS (Table 1).

Spatial variability of H_2O vapour above the cloudtops was detected by PVO/VORTEX (Schofield et al., 1982). On the nightside, the H_2O abundance was below the detection limit (6 ppm). The equatorial mid-afternoon was the wettest (up to 100±40 ppm *vs.* < 6–30 ppm elsewhere). This enhancement may have been associated with vertical uplift of deeper, moister air via convection and Hadley circulation.

Below the clouds, conflicting water abundance results have been reported from different instruments on the PVO, Venera and Vega probes. However, the low water vapour abundances found by the Venera spectrophotometer experiments (Ignatiev et al., 1997) were confirmed by the PVO mass spectrometer (Donahue & Hodges, 1992, 1993) and also supported by Earth-based IR spectroscopy (Bézard et al., 1990; de Bergh et al., 1995; Meadows & Crisp 1996). For example, the Earth-based 1.18 μm spectra of Meadows & Crisp (1996) are best fitted by a profile with 20±15 ppmv H_2O at the 47 km altitude cloud base, increasing to 45±15 ppmv at 30 km, and remaining constant at that value down to the surface. Similarly, NIMS data at 1.18 μm give an H_2O mixing ratio of 30±15 ppmv in the lowest 10 km (Drossart et al., 1993). While NIMS showed no horizontal variation exceeding the 20% level over its sparse sampling of 30 sites, intriguing hints of 10% variability remain. Near-IR observations of water vapour in the spectral windows near 1.10, 1.18, 1.74 and 2.4 μm by PFS would have provided opportunities to improve dramatically the spatial and temporal coverage of water vapour in the deep atmosphere. Spectra of the 1.10 μm and 1.18 μm windows constrain the water vapour concentrations near the surface, while simultaneous measurements in the 1.74 μm and 2.3 μm windows provide information between 35 km and 45 km, while measurements at longer thermal IR wavelengths constrain the water vapour within and above the clouds.

1.13.2 Clouds and meteorology

PFS will investigate the distribution and variability of the lower and middle clouds to ascertain the growth and dissipation rates of cloud masses and their constituent particles. The Galileo/NIMS 'snapshot' of the pole-to-pole distribution of cloud particles found large variations in mean particle size, with marked hemispherical asymmetry (Carlson et al., 1993a). In particular, particles were found to be 10 times larger (by volume) in the northern hemisphere compared to the southern (Fig. 3).

Explanations for such marked hemispherical differences in cloud particle sizes are uncertain, but likely involve spatial variations in dynamical properties such as temperature, eddy diffusion (turbulence) and strengths of up/downdrafts bringing cloud-forming gases (principally SO_2 and H_2O) into the region. If cloud particle size is due to mixing of vertically stratified source regions (e.g., photochemical and condensation source mechanisms), then the mixing must be coherent over very large spatial scales, in turn implying relatively small variations in small-scale dynamical regimes. Yet the distinct regional character of particle sizes may indicate sharp regional variations in the strength of dynamical mechanisms, such as turbulence and up/downwelling.

PFS will obtain particle size and cloud column abundance maps of the nightside several times per week in order to observe the temporal growth and decay of clouds and cloud particles. These observations will be correlated with temporally (and spatially) varying abundances of parent gases and with the observed wind and eddy fields to ascertain mechanisms explaining the distinct regional differences in particle size.

2. Instrument Description

2.1 Introduction

PFS is a double-pendulum interferometer working in two wavelength ranges (0.9–5.5 µm and 5.5–45 µm). The Venus radiation is divided into two beams by a dichroic mirror (Fig. 16). The two ranges also correspond to two planes arranged vertically, in which the two interferometers are placed, so that the same motor can simultaneously move the two pendulums and the two channels are sampled simultaneously and independently (Figs. 17 & 18). The pendulum motion is accurately controlled by a laser diode reference channel making use of the same optics as the planet's radiation. The same laser diode also generates the sampling signal for the analogue/digital converter (ADC), thus measuring the displacement of the double-pendulum mirror in 450/4 nm steps. The measurements obtained are double-sided interferograms, so that the Fast Fourier Transform (FFT) can be computed without caring much about the zero optical path difference location.

2.2 Instrument organisation

PFS resulted from the effort of several groups in different countries: Italy, Russia, Poland, Germany, France and Spain. The flight hardware was produced in Italy (mainly the digital electronics controlling the instrument, and the interferometer block with its controlling electronics plus the ground-support equipment for the spacecraft simulator), Poland (power supply and the pointing system), and Russia and Germany (special parts and subassemblies).

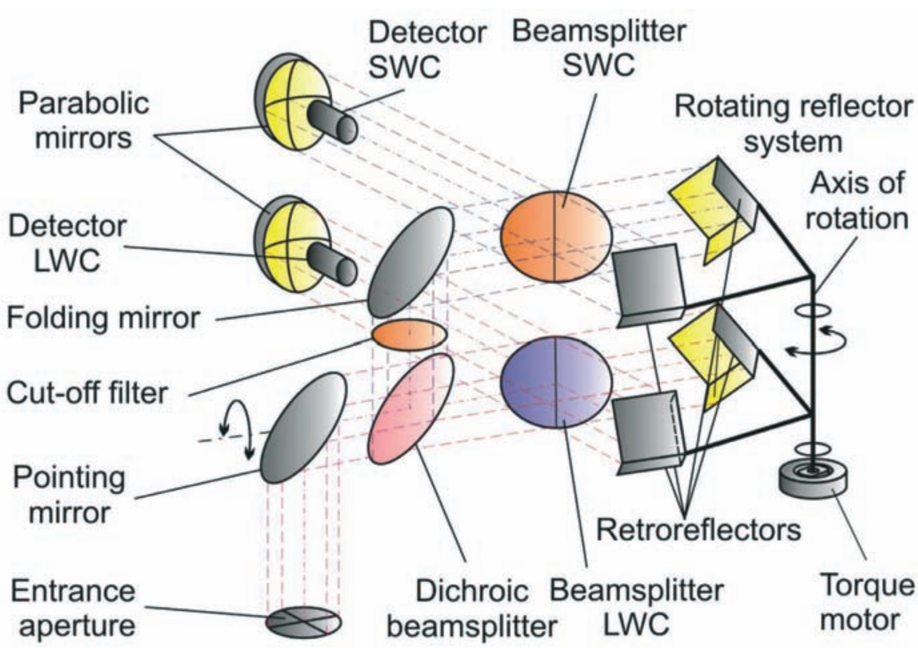

Fig. 16. The PFS optical scheme.

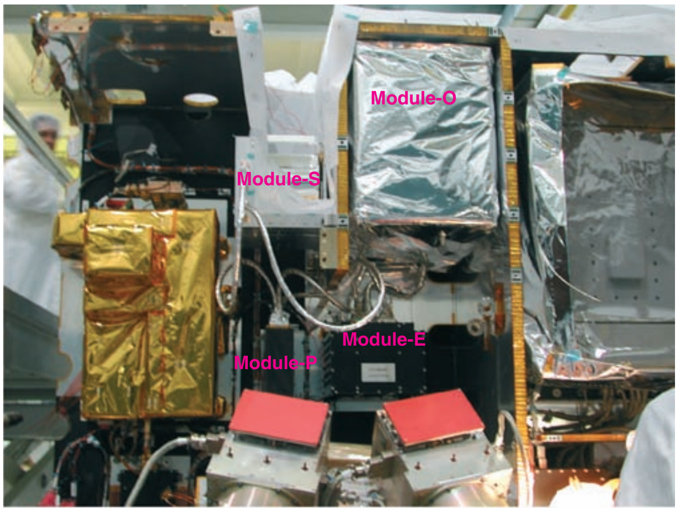

Fig. 17 (above). PFS integrated on the spacecraft.

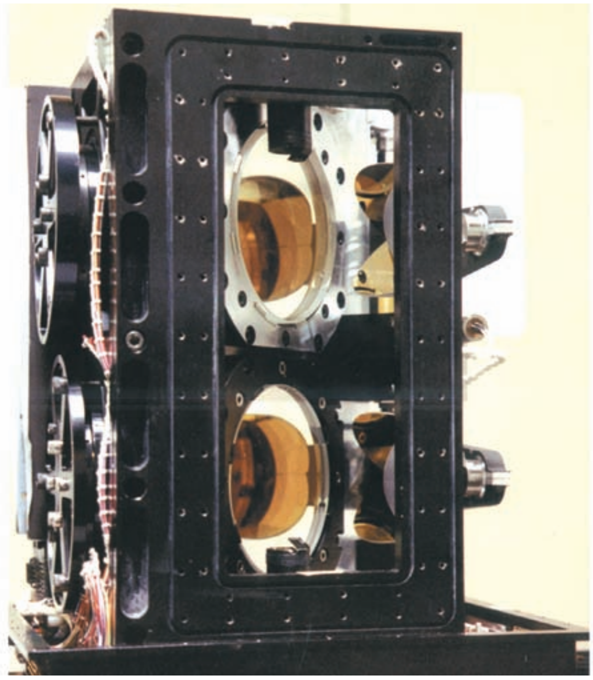

Fig. 18 (right). The core of the PFS double interferometer. The two beam splitters are visible.

2.3 Technical description

The flight hardware, totalling 31.5 kg, is divided into four modules plus their connecting cables. The interferometer ('Module-O'), with its optics and proximity electronics, is the core of the instrument. The pointing device ('Module-S') switches between the radiation from Venus or from the flight calibration sources. The digital electronics ('Module-E') include a 32-Mbit mass memory. The power supply ('Module-P'), with the DC/DC converter, the redundancies and the separate power suppliesfor the 16-bit ADCs.

2.4 Module-O

Module-O is divided into the Interferometer Block (IB) and the Electronics Block (EB). They are mechanically separated but electrically connected through six cables. The highly compact IB is a gas-tight box filled by dry nitrogen in order to preserve the hygroscopic optical elements.

2.4.1 Optical scheme of Module-O

The optical scheme of PFS is shown in Fig. 16. The incident IR beam falls onto the entrance filter that separates the radiation of the SW channel from that of the LW channel and directs each into the appropriate interferometer channel. The Module-S in front of the interferometer allows the FOV to be pointed along and across the projection of the flight path onto the planet's surface. It also directs the FOV at the internal blackbody source diffusers and to open space for inflight calibration. Each PFS channel is equipped with a pair of retroreflectors attached by brackets to an axle rotated by a torque motor. The axle and drive mechanism are used for both channels, which are vertically separated. The optical path difference is generated by the rotation of the retroreflectors (Hirsch & Arnold, 1993). The motor controller uses the outputs of two reference channels, which are equipped with laser diodes. This interferometer design is very robust against misalignment in a harsh environment, in comparison with the classical Michelson-type interferometer (Hirsch, 1997). The detectors are in the centre of the parabolic mirrors. The optical path is changed by rotating the shaft of the double pendulum along its axis. In this way, the optical path is four times that provided by a single cube-corner displacement because two mirrors move at the same time. The dichroic mirror acts as a fork that divides the two spectral ranges. Indeed, it reflects all the wavelengths below 5 µm and remains more or less transparent for longer wavelengths. The band stop for wavelengths below 0.9 µm is provided by the coated window, with its cutoff at 0.9 µm and placed in the optical inlet of the SW channel. This filter is tilted by 1.5° so that the radiation returning to the source is not partially reflected onto the detector.

The double-pendulum axis is rotated by a brushless, frictionless motor (two for redundancy). The shaft of the double pendulum is held only by two preloaded ball bearings so additional mechanical friction is required for stabilising the pendulum speed.

Double-sided interferograms are acquired by placing the zero optical path difference in the centre of the mirror displacement. A double-sided interferogram has several advantages, including a relative insensitivity to phase errors. Bilateral operation is adopted in order to reduce the time-cycle of each measurement, but separate calibration for each direction is recommended in order to maintain the radiometric accuracy.

The reference beam is a diode laser (InGaAsP at 900 nm); its detector is an IR photodiode with maximum response at about 1.2 µm. The beam of the reference channel is processed like the input signal so that its optical path coincides with that of the signal being studied. Each channel has its own reference beam and the different lengths of the double-pendulum arms are fully compensated for. Because the LW beam splitter is not transparent at the wavelength of the corresponding reference diode laser, a special small window was added in order to keep the attenuation of the laser beams negligible through the beam splitter itself. The unused output beams of the two reference channels terminate into optical traps.

2.4.2 Electronics of Module-O

Most of the electronics inside Module-O are analogue but the microprocessor-based On-Board Data Management (OBDM) board controls all the complex procedures during acquisition of the interferogram, including communication with Module-E. It includes 32 kword of EPROM for software storage and 96 kword for data. The most important electronics block is the speed controller. The zero crossing of an interferogram of a monochromatic source that is very stable in wavelength can be used for sampling the interferogram of the source under study. Ideally, the interferogram of the monochromatic source should be a pure sine wave but it is not simply because its interferogram is limited in time. The shorter the wavelength of the reference source means better sampling accuracy.

For PFS, 900 nm is the reference source because of the limited variety of diode lasers and it simplifies the optical design. The wavelength of a diode laser depends on its temperature and power, so great care has to be taken in their control.

The speed of the double pendulum is such that a frequency of 2.5 kHz is generated for the SW channel, so a train of 5 kHz pulses is produced from the electronics of the SW reference channel. Thermal control is also very important for an IR interferometer; heaters and thermometers are positioned at eight locations.

A locking system blocks the double pendulum during launch and manoeuvring for orbital insertion and correction. The procedure of locking and unlocking takes a minimum of 3 min but using a paraffin actuator means it can be repeated hundreds of times. The launch acceleration vector was along the axis of the double pendulum for maximum robustness.

The photoconductor SW channel detector can work at temperatures down to 200K. It is passively cooled through a radiator and its holder is partially insulated from the rest of the IB. For the LW channel, the pyroelectric detector can operate without performance degradation even at ambient temperatures.

2.5 Module-E

Module-E controls all the PFS modules: the communications to and from the spacecraft, memorising and executing the command words, and operating PFS and sending back the data words to the spacecraft. Moreover, it synchronises all the procedures according to the time schedule and to the clock time from the spacecraft.

2.6 Module-P

PFS combines many kinds of electrical energy consumers: standard digital and analogue electronics, sensitive preamplifiers and ADCs, light sources and electromechanical devices (motors and relays). All of them have different supply requirements and some need to be electrically isolated (to ensure extremely high stability) and/or individually controlled by Module-E's processor ('DAM'). This is why Module-P is more complicated than a simple DC/DC converter: there are three independent converters, six different power outputs (totalling 13 independent voltages), one common input interface to satellite and one interface to DAM. All converters have cold redundancy. Switching between main/reserve +5 V is controlled by the spacecraft, while the other main/reserve converters are controlled by PFS itself.

2.7 Module-S

The pointing system is required to measure not only the planetary radiation but also the calibration blackbody and empty space. As Venus Express is nadir-pointing, Module-S needs only one degree of rotation, simplifying the design and reducing the mass considerably. The mirror can point at: the internal calibration lamp, the internal blackbody and deep space (80º), 25º, 12.5º, 0º, –12.5º, –25º. An 'imaging mode' was introduced, in which 11 positions of the mirror are assumed; for each position a number *n* (programmable) of measurements can be taken. The 11 positions are: 0º, ±2.5º, ±5.0º, ±7.5º, ±10.0º, ±12.5º.

2.8 Modes of operation, data acquisition cycle

Module-S and Module-O work in parallel during an observation session, while Module-E coordinates operations of the other modules by sending commands and receiving messages. During measurements, Module-S must be motionless while Module-O acquires data. This is the only synchronisation point in the data-acquisition cycle. Upon completion of acquisition, all the modules work asynchronously while Module-E coordinates their operations:

— starts rotation of Module-S;
— receives LW and SW interferograms from Module-O;
— prepares the telemetry data pack i.e. splits information into frames and stores them in the mass memory;
— upon completion of the Module-S rotation gives a command to Module-O to start new acquisition.

After each data-acquisition cycle, PFS checks whether new telecommands have been received and, if any, executes them. Telemetry can be sent at any time on request from the spacecraft.

2.9 Inflight calibration

During observation sessions, PFS periodically performs calibrations by sending commands to Module-S to point sequentially at the calibration sources: deep space, calibration lamp and internal blackbody. The housekeeping information obtained from Module-O after each calibration measurement contains, in particular, the temperatures of the sensors and the blackbody. These data are used for the computation of the absolute spectra for the LW channel.

3. Test and Calibration

3.1 What is measured

The two detectors of the LW and SW channels measure the light intensity of the two interferograms. The repetition of the measurement while the double pendulum moves at constant speed gives the interferogram. In order to compute the spectrum from the interferogram, the measurements must be taken at constant optical path difference, information given by the zero crossings of the sine signal from the interferogram of a monochromatic light (the laser diode).

3.2 Responsivity and signal-to-noise ratios

'Calibration' in this context means laboratory studies of the instrument properties that are necessary (although perhaps not sufficient) to extract spectra in absolute units from the observations of Venus by PFS. Ideally, calibrations should result in the algorithm of transfer from telemetric information to spectra of Venus in absolute units. However, instrument properties are not constant with time and the problem is complicated by the differences between laboratory and space conditions. Additional information, including inflight calibration and even models of Venus spectra, is necessary for processing actual data.

Having a set of ν independently found $B_{\nu 0}(i)$ spectra, we can compute the average spectrum $\mathbf{B}_{\nu 0}$ and noise equivalent brightness (NEB)

$$\mathrm{NEB}_{\nu}^{2} = \sum \frac{\mathrm{B}_{\nu 0}(i) - \mathbf{B}_{\nu 0}}{n-1}$$

Two blackbody sources (cooled by liquid nitrogen) were used to study the LW channel properties; an integrating sphere source and a blackbody at 1400K were used to study the SW channel (Fig. 19). Sensitivity D_ν and NEB_ν were then computed from these measurements. The spectral resolution was measured with a mercury lamp and taking spectra with known features.

Rough computations show that a signal-to-noise ratio at Venus of about 100 or larger would be achieved in the vicinity of the 15 μm bands with the detector at 284K (Fig. 20). This is good enough for retrieving the vertical temperature profiles of the atmosphere. Further study of the thermal behaviour was necessary and was done in space. It is evident from Fig. 21 that the noise-equivalent

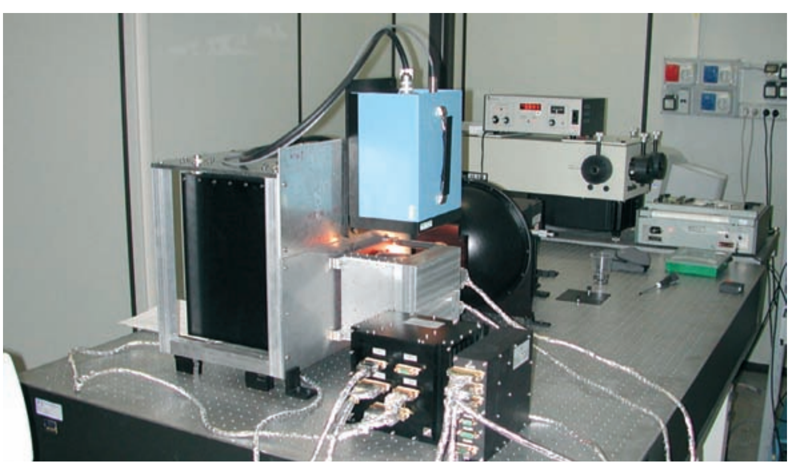

Fig. 19. PFS during calibration. A blackbody and an integrating sphere were used.

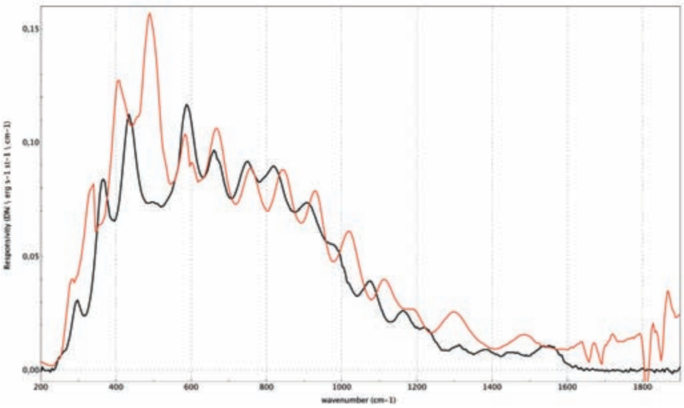

Fig. 20. LW channel responsivity for Mars Express (red) and for Venus Express (black).

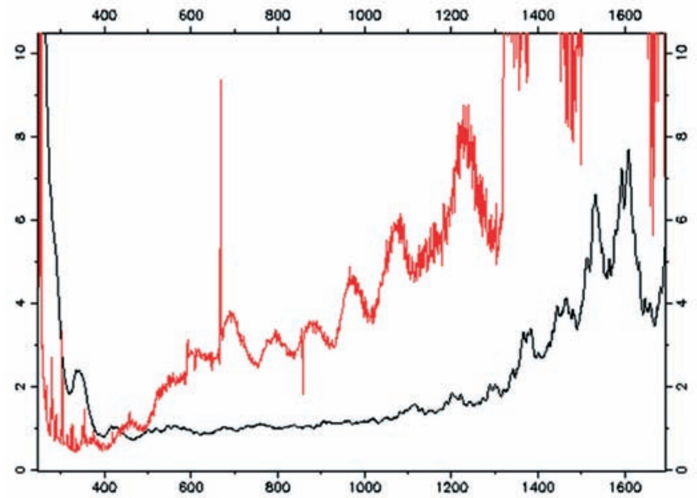

Fig. 21. NER for the LW channel for Mars Express (red) and Venus Express (black).

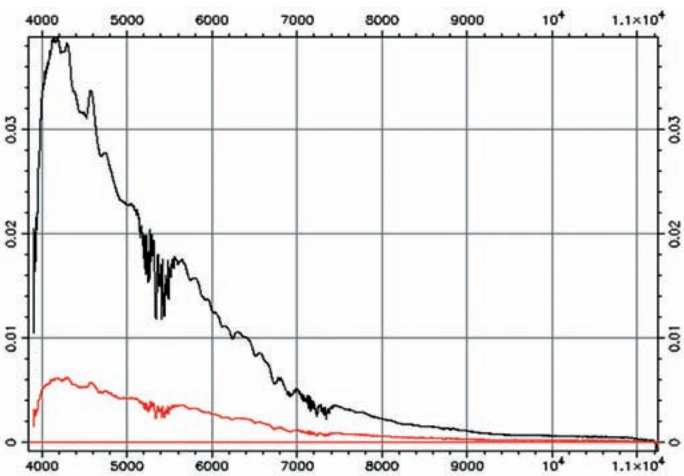

Fig. 22. Responsivity of the solar part of the SW channel: dayside (red) and nightside (black).

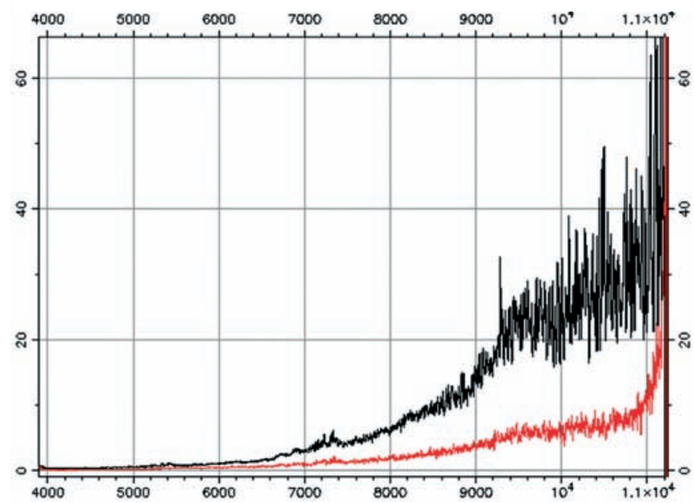

Fig. 23. NER of the SW channel in the solar part: dayside mode (black) and nightside mode (red).

radiance (NER) for the LWC was lower than on Mars Express, probably due to the improved performance of the beam splitter.

The responsivity of the SW channel is given in Fig. 22 for the solar part; the NER is given in Fig. 23. Two curves are given: one for the dayside mode and one for the nightside mode (different attenuation or gain factors.) From Fig. 22, it seems that for wavenumbers $\nu > 8000\ cm^{-1}$ the responsivity is rather poor. The reason is that the semitransparent mirror separating the LW and SW radiation has low reflectivity in this region; this is also the part of the spectrum where losses through optical misalignment are greater. In reality, the situation is much better than it appears from these figures. In order to test the actual performance, PFS was pointed out of the laboratory window to measure the spectrum of the Earth's atmosphere (section 3.3).

3.3 Examples of measurements

Room-temperature measurements were made by looking out of the open window

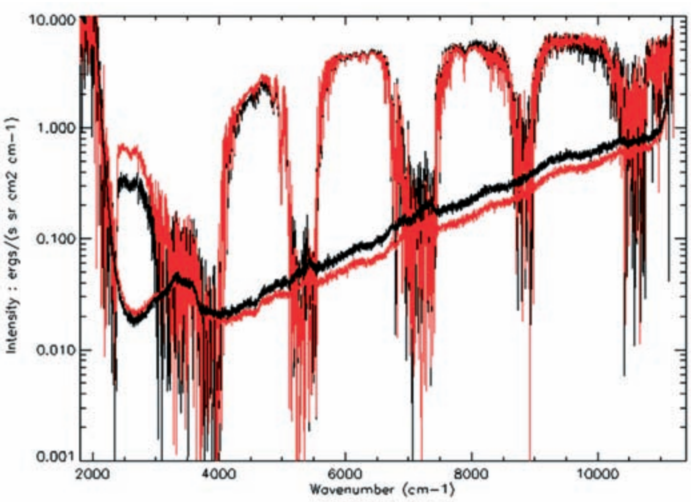

Fig. 24. SW spectrum of the Earth's atmosphere: dayside mode (black), nightside mode (red). The oblique curve gives the NER.

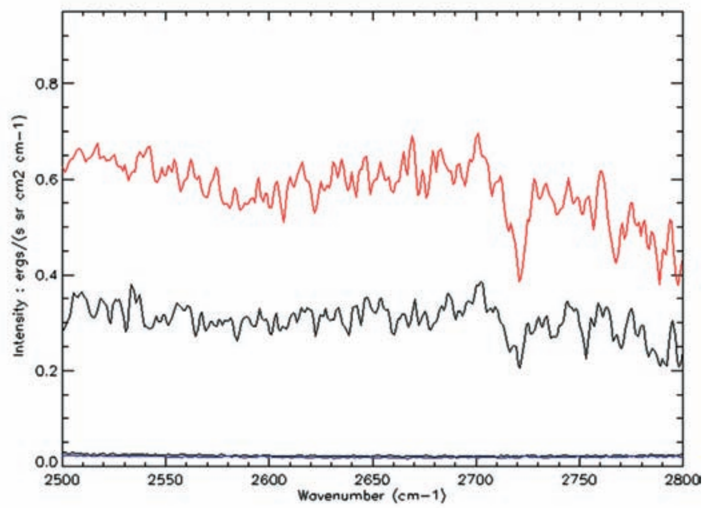

Fig. 25. The HDO line in PFS measurements of Earth's atmosphere: nightside mode (red), dayside mode (black).

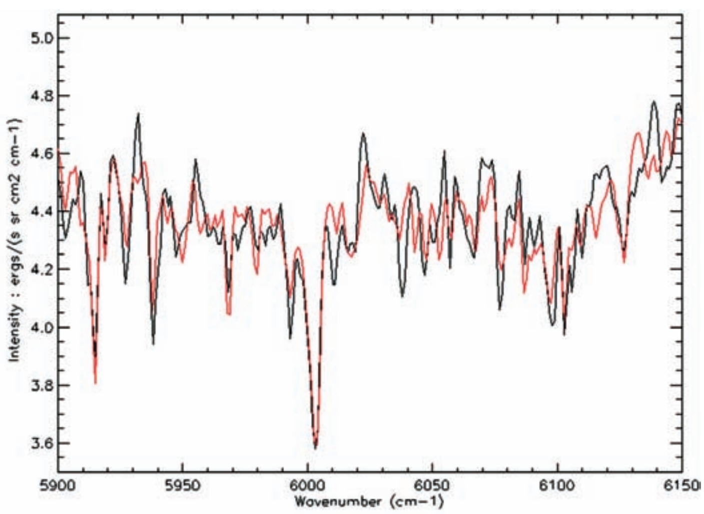

Fig. 26. Methane in the Earth's atmosphere measured by PFS. Enlargement of Fig. 24.

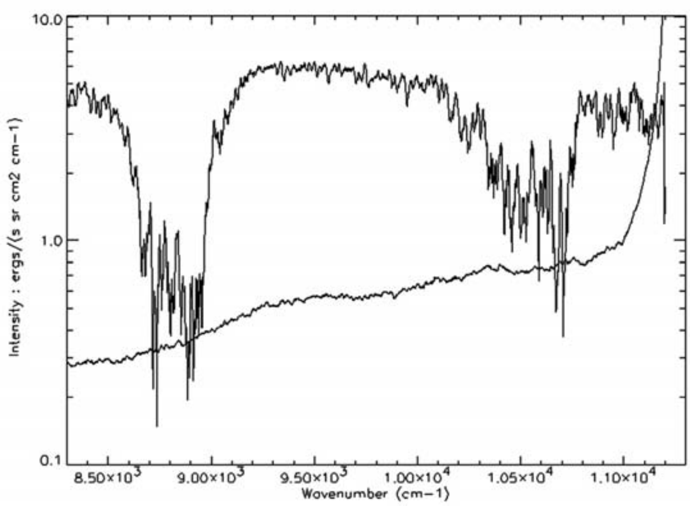

Fig. 27. Enlargement of Fig. 24. in a spectral region not available to the PFS of Mars Express. Two new water bands are observed. Data are smoothed over 15 points.

of the institute towards distant mountains. Figure 24 shows the entire measured spectrum from 2000 cm^{-1} to 11 400 cm^{-1}. Data were acquired in two different modes: dayside (signal attenuation by a factor of 8), and nightside (amplification by 8). The data are shown calibrated. The measured NER is also shown separately for the two measurements. Enlargements of portions of these measured spectra are given in Fig. 25 for the HDO line, Fig. 26 for the oxygen line and Fig. 27 for the spectral interval added for Venus Express (8000–11 400 cm^{-1}, absent for Mars Express). The results show that, by averaging a few measurements, the SNR can be increased to achieve all the scientific objectives.

4. Data-taking Along the Orbit

4.1 Data transmission modes

Data transmission modes (DTMs) 1–28 define the type of scientific data that PFS selects and stores in the mass memory to be sent to the Earth; 17 and 18 are the most used. Mode 0 is used for the PFS autonomous test. For any science

DTM, PFS acquires both LW and SW interferograms then selects the required data. Interferograms can be selected either completely or in half (the central part) or quasi-one sided, giving reduced resolution.

There are 10 defined scientific DTMs:

— MODE 17: full interferograms (4500 points in the LW channel and 22 500 points in the SW channel);
— MODE 2: full LW interferograms;
— MODE 18: full SW interferograms;
— MODE 4: reduced resolution interferograms;
— MODE 5: reduced resolution LW interferograms;
— MODE 6: reduced resolution SW interferograms;
— MODE 8: partial LW and partial (one-sided right) SW interferogram (3500 points in the LW channel and 12 250 points in the SW channel);
— MODE 7: full LW and partial (one-sided right) SW interferogram (4500 points in the LW channel and 12 250 points in the SW channel);
— MODE 28: partial LW and partial (one-sided left) SW interferogram (3500 points in the LW channel and 12 250 points in the SW channel);
— MODE 27: full LW and partial (one-sided left) SW interferogram (4500 points in the LW channel and 12 250 points in the SW channel).

The most-used mode, as for Mars Express, was planned to be Mode 17 – the full interferogram mode.

4.2 Data taking along the orbit

PFS was intended to take spectra when the altitude was lower than 20 000 km. A typical sequence is:

— apocentre: PFS is off.
— pericentre – 60 min: switch on; wait for warm-up; start autonomous test; calibration LW; calibration SW; calibration deep space. Scanner in nadir direction. Give data to the spacecraft.
— pericentre – 45 min, start observations. Give data to the spacecraft.
— pericentre +45 min, stop observations. Give data to the spacecraft.
— pericentre +46 min: calibration LW; calibration SW; calibration deep space. Autonomous test. Give data to satellite. Switch off.
— up to apocentre off.

The spacecraft limitation for internal data transmission averages 32 Kbit/s. In total, 60 calibration measurements per orbit were planned, in addition to the 460 Venus measurements.

References

Allen, D.A. & Crawford, J.W. (1984). Cloud Structure on the Dark Side of Venus. *Nature* **307**, 222–224.

Atreya, S.K. (1986). *Atmospheres and Ionospheres of the Outer Planets and their Satellites*. Springer-Verlag, New York-Berlin, pp93–95 and pp82–88 in Chapter 5.

Avduevskiy, V.S., Marov, M.Ya., Kulikov, Yu.N., Shari, V.P., Gorbachevskiy, A.Ya., Uspenskiy, G.R. & Cheremukhina, Z.P. (1983). Structure and Parameters of the Venus Atmosphere According to Venera Probe Data. In *Venus* (Eds. D.M. Hunten, L. Collin, T.M. Donahue & V.I. Moroz), Univ. of Arizona Press, Tucson, USA, pp681–765.

Baines, K.H. & Carlson, R.W. (1991). Galileo/NIMS at Venus: Middle-Atmosphere Zonal and Meridional Winds, and Implications for the Observed Mid-Level Cloud Morphology. *BAAS* **23**, 1995–1998.

Baines, K.H., Bellucci, G., Bibring, J.-P., Brown, R.H., Buratti, B.J., Bussoletti, E., Capaccioni, F., Cerroni, P., Clark, R.N., Cruikshank, D.P., Drossart, P., Formisano, V., Jaumann, R., Langevin, Y., Matson, D.L., McCord, Thomas, B., Mennella, V., Nelson, R.M., Nicholson, P.D., Sicardy, B., Sotin, C., Hansen, G.B., Aiello, J.J. & Amici, S. (2000). Detection of Sub-micron Radiation from the Surface of Venus by Cassini/VIMS. *Icarus* **148**, 307–311.

Barsukov, V.L., Basilevsky, A.T., Volkov, V.P., Zharkov, V.N. (Eds.) (1992). *Venus Geology, Geochemistry, and Geophysics, Research Results from the USSR*, The University of Arizona Press, Tucson-London.

Bertaux, J.-L. Widemann, T., Hauchecorne, A., Moroz, V.I. & Ekonomov, A.P. (1996). VEGA-1 and VEGA-2 Entry Probes: An Investigation of Local UV Absorption (220-400 nm) in the Atmosphere of Venus (SO_2, Aerosols, Cloud Structure). *J. Geophys. Res.* **101**, 12709–12745.

Bézard, B., deBergh, C., Crisp, D. & Maillard, J-P. (1990). The Deep Atmosphere of Venus Revealed by High-Resolution Nightside Spectra. *Nature* **345**, 508–511.

Bézard, B., deBergh, C., Fegley, B., Maillard, J.-P., Crisp, D., Owen, T., Pollack, J.B. & Grinspoon, D. (1993). The Abundance of Sulfur Dioxide below the Clouds of Venus. *Geophys. Res. Lett.* **20**, 1587–1590.

Bjoraker, G.L., Larson, H.P., Mumma, M.J., Timmermann, R. & Montani, J.L. (1992). Airborne Observations of the Gas Composition above the Cloud Tops: Measurements of H_2O, HDO, HF and the D/H and $^{18}O/^{16}O$ isotopic ratios. *Bull. Amer. Astron. Soc.* **24**, 995.

Bougher, S.W., Hunten, D.M. & Phillips, R.J. (Eds.) (1997). *Venus II*. The University of Arizona Press, Tucson, Arizona, USA.

Carlson, R.W., Baines, K.H., Encrenaz, Th., Taylor, F.W., Drossart, P., Kamp, L.W., Pollack, J.B., Lellouch, E., Collard, A.D., Calcutt, S.B., Grinspoon, D., Weissman, P.R., Smythe, W.D., Ocampo, A.C., Danielson, G.E., Fanale, F.P., Johnson, T.V., Kieffer, H.H., Matson, D.L., McCord, T.B. & Soderblom, L.A. (1991). Galileo Infrared Imaging Spectroscopy Measurements at Venus. *Science* **253**, 1541–1548.

Carlson, R.W., Kamp, L.W., Baines, K.H., Pollack, J.B., Grinspoon, D.H., Encrenaz, Th., Drossart, P. & Taylor, F.W. (1993a). Variations in Venus Cloud Particle Properties: A New View of Venus's Cloud Morphology as Observed by the Galileo Near-Infrared Mapping Spectrometer. *Planet. Space Sci.* **41**, 477–485.

Carlson, R.W., Baines, K.H., Girard, M., Kamp, L.W., Drossart, P., Encrenaz, T. & Taylor, F.W. (1993b). Galileo/NIMS Near Infrared Thermal Imagery of the Surface of Venus. In *Proc. XXIV Lunar & Planetary Science Conf.*, pp253.

Connes, P., Connes, J., Benedict, W.S. & Kaplan, L.D. (1967). Traces of HCl and HF in the Atmosphere of Venus. *Astrophys. J.* **147**, 1230–1237.

Connes, P., Connes, J., Kaplan, L.D. & Benedict, W.S. (1968). Carbon Monoxide in the Venus Atmosphere. *Astrophys. J.* **152**, 731–743.

Connes, P., Connes, J. & Maillard, J.P. (1969). *Atlas des Spectres dans le Proche Infrarouge de Venus, Mars, Jupiter et Saturn.* CNRS, Paris, France.

Connes, P., Noxon, J.F., Traub, W.A. & Carleton, N.P. (1979). O_2 ($^1\Delta$) Emission in the Day and Night Airglow of Venus. *Astrophys J.* **233**, L29–L32.

Crisp, D. & Titov, D.V. (1997). The Thermal Balance of the Venus Atmosphere. In *Venus II* (Eds. S.W. Bougher, D.M. Hunten & R.J. Phillips), The University of Arizona Press, Tucson, Arizona, USA, pp353–384.

Crisp, D., Sinton, W.M., Hodapp, K.W., Ragent, B., Gerbault, F., Goebel, J., Probst, R., Allen, D. & Pierce, K. (1989). The Nature of the Near-Infrared Features on the Venus Night Side. *Science* **253**, 1263–1267.

Crisp, D., Allen, D., Grinspoon, D.H. & Pollack J.B. (1991a). The Dark Side of Venus: Near-Infrared Images and Spectra from the Anglo-Australian Observatory. *Science* **253**, 1263–1267.

deBergh, C., Bézard, B., Owen, T., Crisp, D., Maillard, J.-P. & Lutz, B.L. (1991). Deuterium on Venus: Observations from Earth. *Science* **251**, 547–549.

deBergh, C., Bézard, B., Crisp, D., Maillard, J.-P., Owen, T., Pollack, J. & Grinspoon, D. (1995). The Water Abundance in the Deep Atmosphere of Venus from High-Resolution Spectra of the Night Side. *Adv. Space Res.* **15**, 79–88.

Dobrovolskis, A.R. (1993). Atmospheric Tides on Venus. IV. Topographic Winds and Sediment Transport. *Icarus* **103**, 276–289.

Donahue, T.M. & Hodges, R.R. (1992). Past and Present Water Budget of Venus. *J. Geophys. Res.* **97**, 6083–6091.

Donahue, T.M. & Hodges, R.R. (1993). Venus Methane and Water. *Geophys. Res. Lett.* **20**, 591–594.

Drossart, P., Bézard, B., Encrenaz, Th., Lellouch, E., Roos, M., Taylor, F.W., Collard, A.D., Calcutt, S.B., Pollack, J., Grinspoon, D.H., Carlson, R.W., Baines, K.H. & Kamp, L.W. (1993). Search for Spatial Variations of the H_2O Abundance in the Lower Atmosphere of Venus from NIMS-Galileo. *Planet. Space Sci.* **41**, 495–504.

Esposito, L.W., Knollenberg, R.G., Marov, M.Ya., Toon, R.B. & Turko, R.P. (1983). The Clouds and Hazes of Venus. In *Venus* (Eds. D.M. Hunten, L. Colin, T.M. Donahue & V.I. Moroz), The University of Arizona Press, Tucson, Arizona, USA, pp484–458.

Esposito, L.W., Bertaux, J.-L., Krasnopolsky, V., Moroz, V.I. & Zasova, L.W. (1984). Chemistry of Lower Atmosphere and Clouds. In *Venus II* (Eds. S.W. Bougher, D.M. Hunten & R.J. Phillips), The University of Arizona Press, Tucson, Arizona, USA, pp415–458.

Gelman, B.G., Zolotukhin, V.G., Lamonov, N.I., Levchuk, B.V., Lipatov, A.N., Mukhin, L.M., Nenarokov, D.F., Rotin, V.A. & Okhotnikov, B.P. (1979). Analysis of the Chemical Composition of the Venusian Atmosphere aboard Venera 12 by Means of a Gas Chromatograph, *Kosmicheskie Issledovaniia* **17**, 708–713. (In Russian.)

Grinspoon, D.H. (1993) Implications of the High D/H Ratio for the Sources of Water in Venus' Atmosphere. *Nature* **363**, 428–431.

Grinspoon, D.H., Pollack, J.B., Sitton, B.R., Carlson, R.W., Kamp, L.W., Baines, K.H., Encrenaz, Th. & Taylor, F.W. (1993). Probing Venus's Cloud Structure with Galileo-NIMS. *Planet. Space Sci.* **41**, 515–542.

Hashimoto, G.L. & Imamura, T. (2001). Elucidating the Rate of Volcanism on Venus: Detection of Lava Eruptions using Near-Infrared Observations. *Icarus* **154**, 239–243.

Hashimoto, G.L. & Sugita, S. (2003). On Observing the Compositional Variability of the Surface of Venus using Nightside Near-Infrared Thermal Radiation. *JGR-Planets* **108**(E9), 5109, doi:10.1029/2003JE002082,2003.

Hirsch, H. (1997). Optical Design and Performance of the Planetary Fourier Spectrometer. *Microchimica Acta* **14** (suppl.), 571–574.

Hirsch, H. & Arnold, G. (1993). Fourier Transform Spectroscopy in Remote Sensing of Solid Planetary Surfaces. *Vib. Spectrosc.* **5**, 119–123.

Hunten, D.M., Colin, L., Donahue, T.M. & Moroz, V.I. (Eds.) (1983). *Venus*, The University of Arizona Press, Tucson, Arizona, USA.

Huntress, W.H., Moroz, V.I. & Shevalev, I.L. (2003). Lunar and Planetary Robotic and Exploration Missions in the 20th Century. *Space Sci. Rev.* **107**, 541-649.

Ignatiev, N.I., Moroz, V.I., Moshkin, B.E., Ekonomov, A.P., Gnedykh, V.I., Grigoriev, A.V. & Khatuntsev, I.V. (1997). Water Vapour in the Lower Atmosphere of Venus: A New Analysis of Optical Spectra Measured by Entry Probes. *Planet. Space Sci.* **45**, 427–438.

Ignatiev, N.I., Moroz, V.I., Zasova, L.V. & Khatuntsev, I.V. (1999). Water Vapor in the Middle Atmosphere of Venus: An Improved Treatment of the Venera 15 IR Spectra. *Planet. Space Sci.* **47**, 1061–1075.

Jenkins, V.M. & Steffes, P.J. (1991). Results for 13-cm Absorptivity and H_2SO_4 Abundance Profiles from Season 10 (1986) Pioneer Venus Orbiter Radio Occultation Experiment. *Icarus* **90**, 129–138.

Jenkins, V.M., Steffes, P.G., Hinson, D.P., Twicken, J.D., Tyler, G.L. (1994). Radio Occultation of the Venus Atmosphere with the Magellan Spacecraft. 2. Results from the October 1991 Experiment. *Icarus* **111**, 79–94.

Klose, K.B., Wood, J.A. & Hashimito, A. (1992). Mineral Equilibria and the High Reflectivity of Venus Mountaintops. *J. Geophy. Res.* **97**, 16353–16369.

Kliore, A.J., Moroz, V.I. & Keating, G.M. (Eds.) (1985). The Venus Reference Atmosphere, *Adv. Space Res.* **5** N11, 1–303.

Krasnopolsky, V.A. (1982). *Photochemistry of the Atmospheres of the Mars and Venus,* Springer Verlag, Berlin-Heidelberg-New York-Tokyo.

Kuiper, G.P. (1962). Infrared Spectra of Stars and Planets. 1. Photometry of Infrared Spectrum of Venus, 1-2.5 microns. *Comm. Lunar. Planet. Lab.* **1**, 83–117.

Kuiper, G.P. & Forbes, F.F. (1967). High Altitude Spectra from NASA CV990 Jet. 1. Venus, 1-2.5 microns, Resolution 20 per cm. *Comm. Lunar. Planet. Lab.* **6**, 177–189.

Kuzmin, A.D. & Marov, M.Ya. (1974). *Physics of the Planet Venus* (in Russian), Moscow, Nauka.

Lecaucheux, J.A., Drossart, P., Laques, P., Deladrierre, F., Colas, F. (1993). Detection of the Surface of Venus on 1 μm from Ground Based Observations. *Planet. Space Sci.* **41**, 543–550.

Linkin, V.M., Blamont, J., Devyatkin, S.I., Ignatova, S.P., Kerzhanovich, V.V., Lipatov, A.N., Malik, K., Stadnyk, B.I., Sanotskii, Ya.V., Stolyarchuk, P.G., Terterashvili, A.V., Frank, G.A. & Khlyustova, L.I. (1987). Thermal Structure of the Atmosphere of Venus from the Results of Measurements taken by Landing Vehicle Vega-2. *Cosmic Res.* **25**, 501–512.

Meadows, V.S., Crisp, D. & Allen, D.A. (1992). Ground Based Near-IR Observations of the Surface of Venus. International Colloquium on Venus, LPI Contribution 789, 70–71.

Meadows, V.S. & Crisp, D. (1996). Ground-Based Near Infrared Observations of the Venus Nightside: The Thermal Structure and Water Abundance near the Surface. *J. Geophys. Res.* **101**, 4595–4622.

Moroz, V.I. (2002). Estimates of Visibility of the Surface of Venus from Descent Probes and Balloons. *Planet. Space Sci.* **50**, 287–297.

Moroz, V.I. (1968). *Physics of Planets* (in Russian), Nauka Press, Moscow. English translation published by NASA as TTF-515 in 1968.

Moroz, V.I. (1981). The Atmosphere of Venus. *Space Sci. Rev.* **29**, 3–127.

Moroz, V.I., Ekonomov, A.P., Moshkin, B.E., Revercomb, H.E., Sromovsky, L.A. & Schofield, J.T. (1985a). Solar and Thermal Radiation in the Venus Atmosphere. In *The Venus Reference Atmosphere* (Eds. A.J. Kliore, V.I. Moroz & G.M. Keating), *Adv. Space Res.* **5** N11, 197–232.

Moroz, V.I., Doehler, K., Ustinov, E.A., Schaefer, K., Zasova, L.V., Spaenkuch, D., Diachkov, A.V., Diubua, R., Linkin, V.M. & Oertel, D. (1985b). Infrared Experiment on Venera-15 and Venera-16 Orbiters. 4. Of Analysis of Spectra in the Ranges of H_2O and SO_2 Absorption Bands. (In Russian) *Kosmicheskie issledovanija* **23** N2, 236–247.

Moroz, V.I., Spaenkuch, D., Linkin, V.M., Dohler, W., Matsygorin, I.A., Schafer, K., Zasova, L.V., Oertel, D., Dyachkov, A.V. & Schuster, R. (1986). Venus Spacecraft's Infrared Radiance Spectra and Some Aspects of their Interpretation. *Applied Optics* **25**, 1710–1719.

Moroz, V.I., Huntress, W.H. & Shevalev, I.L. (2002). Planetary Missions of the 20th Century. (In Russian). *Kosmicheskie issledovanija* **40** N5, 451–481.

Pettengill, G.H., Ford, P.G. & Chapman, B.D. (1988). Venus: Surface Electromagnetic Properties. *J. Geophys. Res.* **93**, 14881–14892.

Pettengill, G.H., Ford, P.G. & Simpson, R.A. (1996). Electrical Properties of the Venus Surface from Bistatic Radar Observations. *Science* **272**, 1628–1631.

Pettengill, G.H., Ford, P.G. & Wilt, R.J. (1992). Venus Surface Emission as Observed by Magellan. *J. Geophys. Res.* **97**, 13091–13102.

Pollack J.B. et al. Night infrared light from Venus' night side: A spectroscopic analysis. Icarus 103, 1–42, 1993.

Schofield, J.T., Taylor, F.W. & McCleese, D.J. (1982). The Global Distribution of Water Vapor in the Middle Atmosphere of Venus. *Icarus* **52**, 263–278.

Seiff, A. (1983). Thermal Structure of the Atmosphere of Venus. In *Venus* (Eds. D.M. Hunten, L. Colin, T.M. Donahue & V.I. Moroz), The University of Arizona Press, Tucson, Arizona, USA, pp215–279.

Seiff, A., Schofield, J.T., Kliore, A.J., Taylor, F.W. & Limaye, S.S. (1985). Models of the Structure of the Atmosphere of Venus from the Surface to 100 kiliometers Altitude. In *The Venus Reference Atmosphere* (Eds. A.J. Kliore, V.I. Moroz & G.M. Keating), *Adv. Space Res.* **5** N11, pp3–58.

Taylor, F.W., Beer, R., Chahine, M.T., Diner, D.J., Elson, L.S., Haskins, R.D., McCleese, D.J., Martonchik, J.V., Reichley, P.E., Bradley, S.P., Delderfield, J., Schofield, J.T., Farmer, C.B., Froidevaux, L., Leung, J., Coffey, M.T. & Gille, J.C. (1980). Structure and Meteorology of the Middle Atmosphere of Venus: Infrared Remote Sensing from the Pioneer Orbiter. *J. Geophys. Res.* **85**, 7963–8006.

Taylor, F.W., Crisp, D. & Bezard, B. (1997). Near Infrared Sounding of the Lower Atmosphere of Venus. In *Venus II* (Eds. S.W. Bougher, D.M. Hunten & R.J. Phillips), The University of Arizona Press, Tucson, Arizona, USA, pp325–352.

Tikhonov, A.N., Goncharskij, A.V., Stepanov, V.V. & Jagola, A.G. (1990). *Numerical Methods of Solving the Ill-Posed Problems,* (In Russian), Moscow, Nauka.

Titov, D.V., Haus, R. & Shaefer, K. (1992). Thermal Fluxes and Cooling Rates the Venus Atmoshere from Venera 15 Infrared Spectrometer Data. *Adv. Space Res.* **12**, 73–77.

Titov, D.V. (1995). Radiative Balance in the Mesosphere of Venus from the Venera 15 Infrared Spectrometer Results. *Adv. Space Res.* **15**, 73–77.

Twomay, S, Herman, D. & Rabinoff, R. (1977). An Extention of Chahine Method of Inverting the Radiative Transfer Solution Equation. *J. Atm. Sci.* **34**, 1085–1093.

Von Zahn, U., Kumar, S., Niemann, N. & Prinn, R. (1983). Composition of the Venus Atmosphere. In *Venus* (Eds. D.M. Hunten, L. Colin, T.M. Donahue & V.I. Moroz), The University of Arizona Press, Tucson, Arizona, USA, pp299–430.

Von Zahn, U. & Moroz, V.I. (1985). Composition of the Venus Atmosphere below 100 km Altitude. In *The Venus Reference Atmosphere* (Eds. A.J. Kliore, V.I. Moroz & G.M. Keating), *Adv. Space Res.* **5** N11, pp173–196.

Wilson, E.H. & Atreya, S.K. (2003). Chemical Sources of Haze Formation in Titan's Atmosphere. *Planet. Space Sci.* **51**, 1017–1033.

Yung, Y.L. & DeMore, W.B. (1982). Photochemistry of the Stratosphere of Venus: Implications for Atmospheric Evolution. *Icarus* **51**, 197–212.

Zasova, L.V., Spaenkuch, D., Moroz, V.I., Schaefer, K., Ustinow, E.A., Doehler, W., Linkin, V.M., Oertel, D., Diachkov, A.V. & Becker-Ross, H. (1985). Infrared Experiment on Venera-15 and Venera-16 Orbiters. Some Conclusions about Structure of Clouds Based on the Analysis of Spectra. (In Russian.) *Kosmicheskie issledovanija* **23**, 221–235.

Zasova, L.V. & Moroz, V.I. (1992). Latitude Structure of the Upper Clouds of Venus. *Adv. Space Res.* **12**, 79–90.

Zasova, L.V., Moroz, V.I., Esposito, L.W. & Na, C.Y. (1993). SO_2 in the Middle Atmosphere of Venus: IR Measurements from Venera-15 and Comparison to UV data. *Icarus* **105**, 92–109.

Zasova, L.V. (1995). The Structure of the Venusian Atmosphere at High Latitudes. *Adv. Space Res.* **16**, 89–98.

Zasova, L.V. & Khatuntsev, I.V. (1997). Thermal Zonal Wind in the Venus Middle Atmosphere According to Venera 15 IR-Spectrometry. *Adv. Space Res.* **19** N8, 1181–1190.

Zasova, L.V., Khatountsev, I.V., Moroz, V.I. & Ignatiev, N.I. (1999). Structure of the Venus Middle Atmosphere: Venera 15 IR Fourier Spectrometry Data Revisited. *Adv. Space Res.* **23** N9, 1559–1568.

Zasova, L.V., Khatuntsev, I.V. & Linkin, V.M. (2000). Zonal Wind in the Middle Atmosphere of Venus. *Cosmic Res*. **38**, 1–49.

Zasova, L.V., Khatuntsev, I.V., Ignatiev, N.I. & Moroz, V.I. (2002). Local Time Variations of the Middle Atmosphere of Venus: Solar-Related Structures. *Adv. Space Res.* **299** N2, 243–248.